

CTCF knockout in zebrafish induces alterations in regulatory landscapes and developmental gene expression

Martin Franke

CABD - CSIC

Elisa de la Calle-Mustienes

Centro Andaluz de Biología del Desarrollo

Ana Neto

Centro Andaluz de Biología del Desarrollo

Rafael Acemel

CABD - CSIC

Juan Tena

Centro Andaluz de Biología del Desarrollo <https://orcid.org/0000-0001-8165-7984>

José Santos-Pereira (✉ jmsanper1@upo.es)

CABD - CSIC <https://orcid.org/0000-0003-3949-0644>

José Luis Gómez-Skarmeta

Centro Andaluz de Biología del Desarrollo (CABD)

Article

Keywords: DNA-binding Protein, Transcriptional Repressor and Insulator, 3D Genome Folding, Chromatin Looping, Enhancer-promoter Interactions, Embryo Patterning and Organogenesis

Posted Date: December 3rd, 2020

DOI: <https://doi.org/10.21203/rs.3.rs-104001/v1>

License: © ⓘ This work is licensed under a Creative Commons Attribution 4.0 International License.

[Read Full License](#)

Version of Record: A version of this preprint was published at Nature Communications on September 13th, 2021. See the published version at <https://doi.org/10.1038/s41467-021-25604-5>.

1
2
3
4
5
6
7
8
9
10
11
12
13
14
15
16
17
18
19
20
21
22
23
24

CTCF knockout in zebrafish induces alterations in regulatory landscapes and developmental gene expression

Martin Franke[#], Elisa De la Calle-Mustienes[#], Ana Neto, Rafael D. Acemel, Juan J. Tena, José M. Santos-Pereira^{*} and José L. Gómez-Skarmeta

Centro Andaluz de Biología del Desarrollo (CABD), Consejo Superior de Investigaciones Científicas/Universidad Pablo de Olavide, 41013 Seville, Spain

[#] These authors contributed equally to this work

^{*} Corresponding author:

José M. Santos-Pereira
phone: +34 954 348 687
email: jmsanper1@upo.es

Word count: 4265

Number of figures: 4

25 **CTCF is an 11-zinc-finger DNA-binding protein that acts as a transcriptional repressor**
26 **and insulator as well as an architectural protein required for 3D genome folding¹⁻⁵. CTCF**
27 **mediates long-range chromatin looping and is enriched at the boundaries of**
28 **topologically associating domains, which are sub-megabase chromatin structures that**
29 **are believed to facilitate enhancer-promoter interactions within regulatory landscapes**
30 **⁶⁻¹². Although CTCF is essential for cycling cells and developing embryos^{13,14}, its *in vitro***
31 **removal has only modest effects over gene expression^{5,15}, challenging the concept that**
32 **CTCF-mediated chromatin interactions and topologically associated domains are a**
33 **fundamental requirement for gene regulation¹⁶⁻¹⁸. Here we link the loss of chromatin**
34 **structure and gene regulation in an *in vivo* model and during animal development. We**
35 **generated a *ctcf* knockout mutant in zebrafish that allows us to monitor the effect of**
36 **CTCF loss of function during embryo patterning and organogenesis. CTCF absence**
37 **leads to loss of chromatin structure in zebrafish embryos and affects the expression of**
38 **thousands of genes, including many developmental genes. In addition, chromatin**
39 **accessibility, both at CTCF binding sites and *cis*-regulatory elements, is severely**
40 **compromised in *ctcf* mutants. Probing chromatin interactions from developmental**
41 **genes at high resolution, we further demonstrate that promoters fail to fully establish**
42 **long-range contacts with their associated regulatory landscapes, leading to altered**
43 **gene expression patterns and disruption of developmental programs. Our results**
44 **demonstrate that CTCF and topologically associating domains are essential to regulate**
45 **gene expression during embryonic development, providing the structural basis for the**
46 **establishment of developmental gene regulatory landscapes.**

47 Vertebrate genomes are folded within the nucleus in a hierarchical manner leading to
48 different levels of chromatin structure that range from chromosome territories to
49 nucleosomes¹⁹⁻²³. At the Kilo- to Megabases scale, chromatin is organized in topologically
50 associating domains (TADs)⁶⁻⁹. According to the current theory, TADs emerge when the
51 cohesin complex, while extruding chromatin, is halted by the CTCF architectural protein^{24,25}.
52 Indeed, acute depletion of CTCF or cohesin in cultured cells lead to a severe loss of TAD
53 insulation or the disappearance of all chromatin loops, respectively^{5,26}. Recent evidences have
54 suggested that TADs facilitate the contact of *cis*-regulatory elements (CREs) with promoters
55 located within them, while preventing interactions with promoters located in neighboring TADs.
56 In this sense, genomic structural variations that rearrange TAD boundaries lead to enhancer-
57 promoter rewiring, alterations in gene expression and congenital malformations²⁷⁻³¹. However,
58 to what extent TADs are crucial for gene regulation is currently under debate. Depletion of
59 CTCF in mammalian *in vitro* systems causes only modest transcriptional alterations^{5,15,32}, in

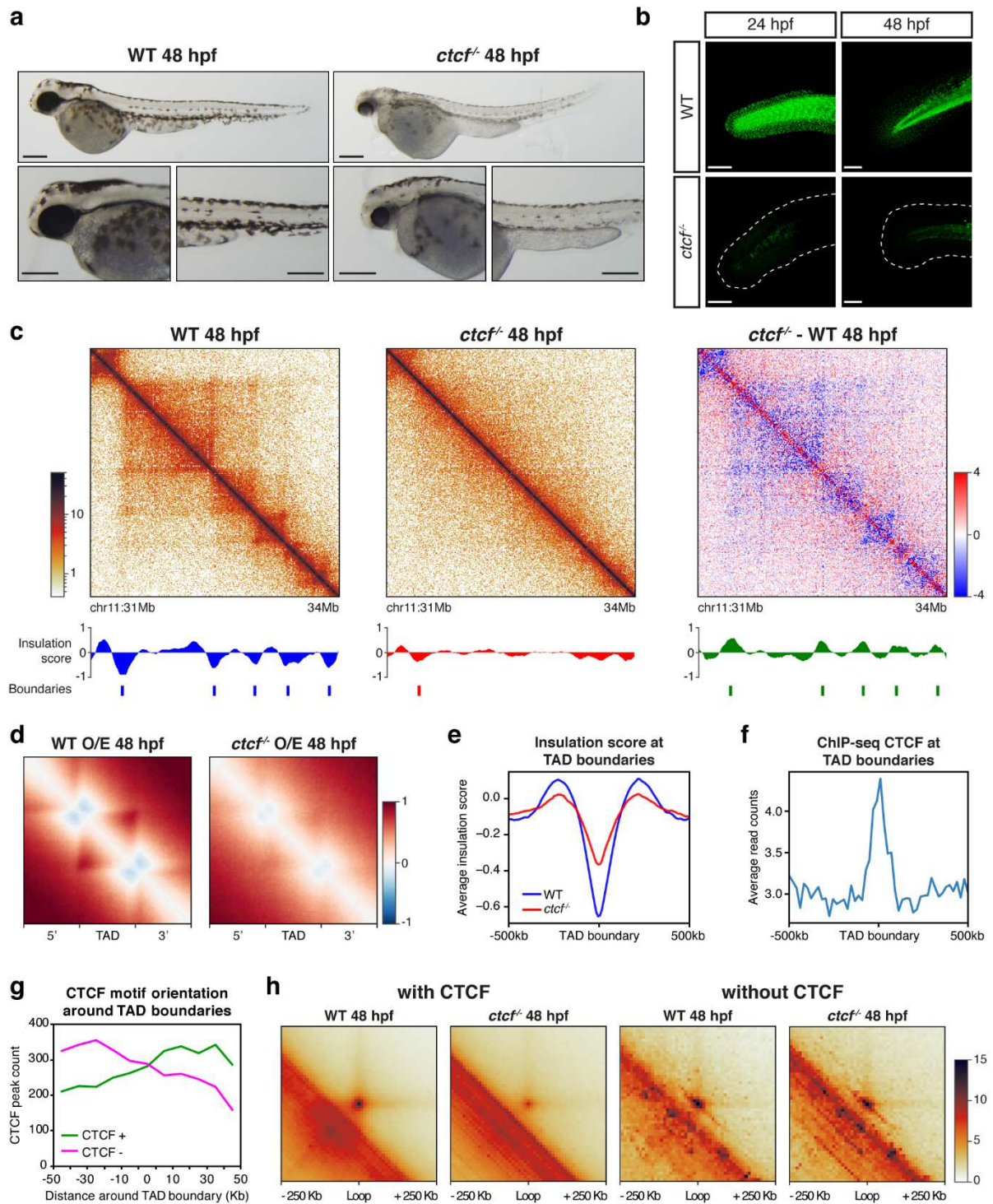
60 agreement with some *in vivo* studies^{33,34}. However, targeted deletion of several CTCF sites
61 and quantitative gene expression analyses reveal loss of gene expression³⁵⁻³⁷. In fact, our
62 understanding of CTCF function *in vivo* during organogenesis is limited to a few physiological
63 contexts due to its essential function during the cell cycle and the early embryonic lethality in
64 mice^{13,14,38,39}. Here, we analyze the genome-wide effect of CTCF knockout in developing
65 zebrafish embryos, showing that chromatin structure is essential for the precise regulation of
66 developmental genes and thus provides a scaffold for the establishment of developmental
67 gene regulatory landscapes.

68

69 **Generation of a zebrafish *ctcf*^{-/-} zygotic mutant**

70 In order to study the requirement of CTCF in an *in vivo* vertebrate model, we have generated
71 a *ctcf* zygotic knockout mutant in zebrafish. Using CRISPR/Cas9 with two single guide RNAs
72 (sgRNAs), we obtained heterozygous *ctcf*^{+/-} adult individuals carrying a 260-bp deletion,
73 encompassing exons 3 and 4 of the *ctcf* gene that leads to a premature stop codon within exon
74 4. The expected truncated CTCF protein is depleted of all zinc finger domains, preventing
75 CTCF binding to chromatin. While *Ctcf*^{-/-} zygotic knockout mice die at peri-implantation
76 stages¹⁴, zebrafish mutants undergo gastrulation and organogenesis and develop normally
77 until pharyngula stages, around 24 hours-post-fertilization (hpf). At 24 hpf, *ctcf*^{-/-} mutants are
78 phenotypically indistinguishable from their heterozygous and wild-type siblings. However, at
79 48 hpf, *ctcf*^{-/-} embryos showed a clear phenotype that included pigmentation defects, heart
80 edema and reduced size of head and eyes (Fig. 1a), dying shortly after this stage.
81 Immunofluorescence analysis of wild-type and *ctcf*^{-/-} mutant embryos showed that CTCF
82 protein was absent both at 24 and at 48 hpf (Fig. 1b), while maternal *ctcf* mRNA is detected at
83 least until 75% of epiboly (8 hpf, gastrulation)⁴⁰. This suggests that the late lethality of zebrafish
84 *ctcf*^{-/-} mutants compared to mice might be due to the presence of maternal CTCF protein for a
85 longer time during early embryonic development. Therefore, our *ctcf*^{-/-} zebrafish mutant
86 provides a unique tool to examine the contribution of this protein in genome architecture, gene
87 expression and body plan formation in a vertebrate model system. We therefore exploited this
88 model using a combination of chromosome conformation capture, transcriptomic and
89 epigenomic techniques.

90



91

92 **Figure 1. Knockout of *ctcf* in zebrafish embryos disrupts chromatin structure.** **a**, Pictures of wild-type (WT)
 93 and *ctcf*^{-/-} zebrafish embryos at 48 hours post fertilization (hpf) showing mutant phenotypes, including reduced size
 94 of head and eyes, heart edema and defective pigmentation. Scale bars represent 250 μ m. **b**, Whole-mount embryo
 95 immunofluorescence of CTCF in WT and *ctcf*^{-/-} zebrafish embryos at 24 and 48 hpf showing the absence of this
 96 protein in the tail and fin fold in knockout mutants. Scale bars represent 100 μ m. **c**, HiC normalized contact maps
 97 at 10 Kb resolution from WT and *ctcf*^{-/-} zebrafish embryos, as well as the difference between them, at 48 hpf. A 3-
 98 Mb genomic region in chr11 is plotted, aligned with the insulation scores and the called topologically associating
 99 domain (TAD) boundaries. **d**, Aggregate analysis of observed/expected HiC signal in WT and *ctcf*^{-/-} embryos at 48
 100 hpf for the 2,438 TADs called in WT embryos, rescaled and surrounded by windows of the same size. **e**, Average
 101 insulation score profiles of WT and *ctcf*^{-/-} zebrafish embryos at 48 hpf around the TAD borders called in the WT. **f**,
 102 Average CTCF ChIP-seq signal in WT embryos at 48 hpf around TAD boundaries. **g**, CTCF peak count of those
 103 peaks containing CTCF motifs located in the positive (CTCF +) or negative (CTCF -) strands around TAD

104 boundaries, showing a clear preference for CTCF + motifs in the 3' side of the boundary and for CTCF - motifs in
105 the 5' side of the boundary. **h**, Aggregate peak analysis of chromatin loops called by HiCCUPs with or without CTCF
106 binding at 48 hpf.
107

108 **CTCF is required for chromatin organization in zebrafish embryos**

109 We first analyzed whether the absence of CTCF in zebrafish embryos caused loss of chromatin
110 structure, as previously reported in *in vitro* models^{5,15}. For this, we performed HiC experiments
111 in wild-type and *ctcf*^{-/-} whole embryos at 48 hpf and visualized the data at 10-Kb resolution.
112 [Figure 1c](#) shows that chromatin structure was established at this stage in wild-type embryos,
113 similar to previous reports⁴¹, detecting 2,438 TADs based on insulation scores⁴². Other 3D
114 chromatin features commonly detected at this scale, such as loops and stripes, were also
115 observed. In contrast, we found a general loss of chromatin structure in *ctcf*^{-/-} embryos, leading
116 to the detection of only 1,178 TADs and to a reduction of intra-TAD contacts and insulation in
117 wild-type TADs ([Fig. 1c-e](#); [Supplementary Fig. 1a-d](#)). These data confirmed that CTCF is
118 essential for 3D chromosome organization in zebrafish embryos, as described for other
119 vertebrates including mammals and frogs^{5,15,43}. Next, we analyzed A and B compartments in
120 wild-type and *ctcf*^{-/-} embryos and, although we found a similar distribution of AB compartments,
121 we detected increased AB interactions and decreased compartmentalization strength in the
122 mutants ([Supplementary Fig. 1e-g](#)). This contrasts with previous data in cultured cells⁵ and
123 suggests that CTCF may be required for higher order chromatin structure at least in this *in vivo*
124 context.

125 We then profiled CTCF binding to chromatin in zebrafish embryos using ChIPmentation
126 and found that wild-type TAD boundaries were enriched for CTCF binding, 97% of them
127 containing CTCF sites ([Fig. 1f](#); [Supplementary Fig. 2a-b](#)). In addition, the consensus motifs of
128 CTCF at these binding sites around TAD boundaries were preferentially located in a
129 convergent orientation ([Fig. 1g](#)), consistent with previous observations^{6,10,41,44,45}. Next, we
130 called chromatin loops in wild-type embryos and detected 1,297 loops, 90% of which contained
131 CTCF binding sites at least at one of the anchors ([Supplementary Fig. 2](#)). Interestingly,
132 aggregate peak analysis of CTCF-containing chromatin loops showed a marked decrease in
133 intensity in *ctcf*^{-/-} mutants, while 10% of loops without CTCF remained largely unaffected by
134 CTCF loss ([Fig. 1h](#)), suggesting that they may be formed by CTCF-independent mechanisms.
135 Therefore, we conclude that CTCF is essential for the establishment of most chromatin loops
136 in zebrafish embryos, similarly to other vertebrates^{5,43}.

137

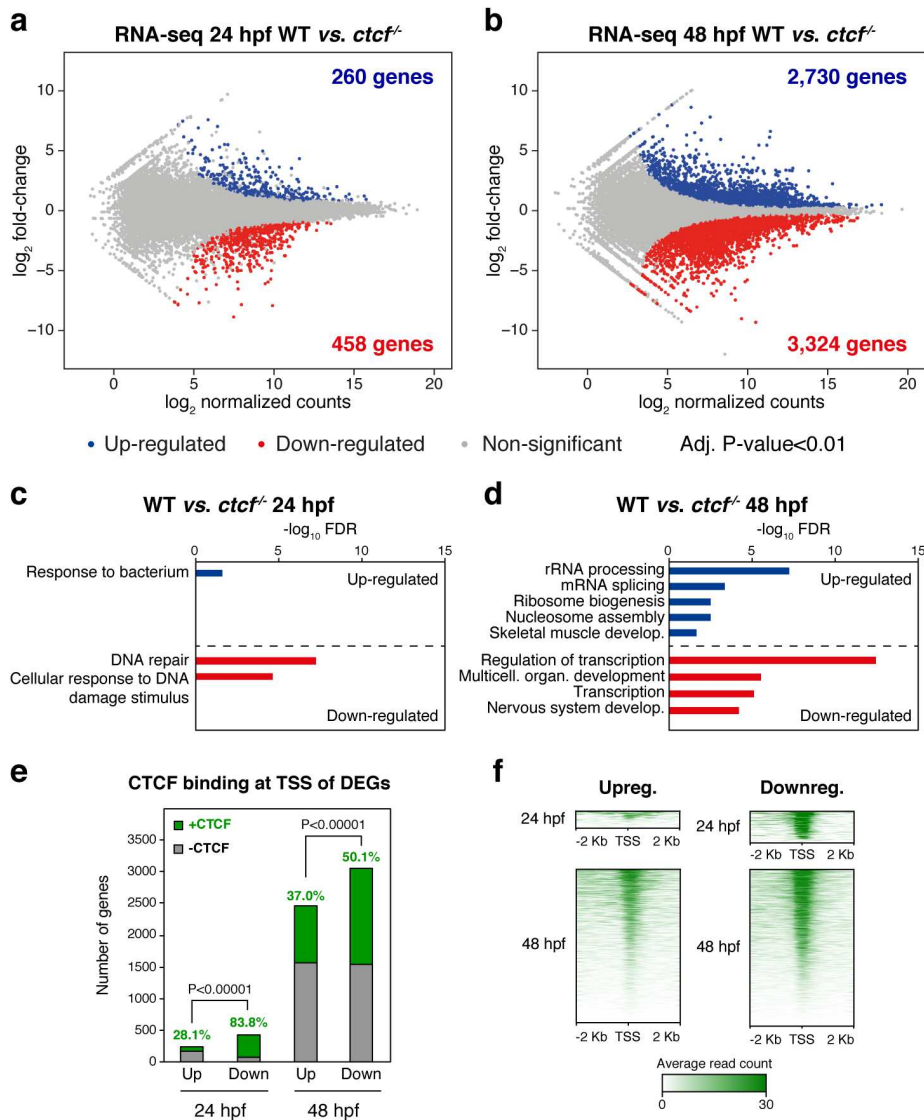
138 **Developmental gene expression requires CTCF**

139 To analyze the effects of CTCF absence over gene expression *in vivo*, we performed RNA-
140 seq on whole embryos at 24 and 48 hpf. At 24 hpf, we detected 260 up- and 458 down-

141 regulated genes (Fig. 2a). However, at 48 hpf, we detected as much as 2,730 up- and 3,324
142 down-regulated genes (Fig. 2b). Strikingly, while differentially expressed genes (DEGs) at 24
143 hpf were enriched only in biological functions related to immune and DNA damage responses,
144 DEGs at 48 hpf were enriched, among other general functions, in transcription regulation and
145 developmental processes including skeletal muscle development or nervous system
146 development (Fig. 2c-d). This indicates that CTCF is required for the expression of thousands
147 of genes during zebrafish development, an impacting result that contrasts to previous
148 observations in *in vitro* experimental setups showing alteration of a few hundred genes upon
149 CTCF removal^{5,32}. Next, we analyzed gene expression changes in the transition from 24 to 48
150 hpf in wild-type embryos and found that genes that get activated in this period tend to be down-
151 regulated in *ctcf*^{-/-} embryos, and vice versa, indicating that many developmental genes fail to
152 acquire their normal expression level during this developmental period (Supplementary Fig. 3).

153 We then explored the possible function of CTCF to directly regulate DEGs by analyzing
154 its binding to their transcription start sites (TSSs). At 24 hpf, we found a clear bias of CTCF
155 binding towards the TSS of down-regulated genes (83.8%) as compared to up-regulated genes
156 (28.1%) (Fig. 2e-f). This confirms previous observations^{5,15} and suggests distinct mechanisms
157 of CTCF function at activated and repressed genes. By contrast, only 50.1% of down-regulated
158 and 37.0% of up-regulated genes at 48 hpf showed CTCF binding at their TSSs (Fig. 2e-f).
159 Interestingly, we observed that down-regulated genes that are enriched in developmental
160 functions were mainly those without CTCF bound at their TSSs (Supplementary Fig. 4), raising
161 the possibility that developmental genes could be de-regulated indirectly due to defects in
162 chromatin folding. Altogether, these data show that CTCF absence leads to altered
163 developmental gene expression that may account for the observed developmental
164 abnormalities.

165



166

167 **Figure 2. CTCF absence in zebrafish embryos leads to altered developmental gene expression.** a-b,
 168 Differential analyses of gene expression between WT and *ctcf*^{-/-} embryos at 24 (a) and 48 hpf (b) from RNA-seq
 169 data (n = 2 biological replicates per condition). The log₂ normalized read counts of WT transcripts versus the log₂
 170 fold-change of expression are plotted. Transcripts showing a statistically significant differential expression (adjusted
 171 P-value < 0.01) are highlighted in blue (up-regulated) or red (down-regulated). The number of genes that correspond
 172 to the up- and down-regulated transcripts are shown inside the boxes. c-d, Gene Ontology (GO) enrichment
 173 analyses of biological processes for up- and down-regulated genes in *ctcf*^{-/-} embryos at 24 (c) and 48 hpf (d). Terms
 174 with a false discovery rate (FDR) < 0.05 are shown and considered as enriched. e, Number of differentially
 175 expressed genes (DEGs) at 24 and 48 hpf showing (green) or not (grey) CTCF binding at their transcription start
 176 sites (TSSs). f, Heatmaps showing CTCF ChIP-seq signal around the TSS of DEGs at 24 and 48 hpf.

177

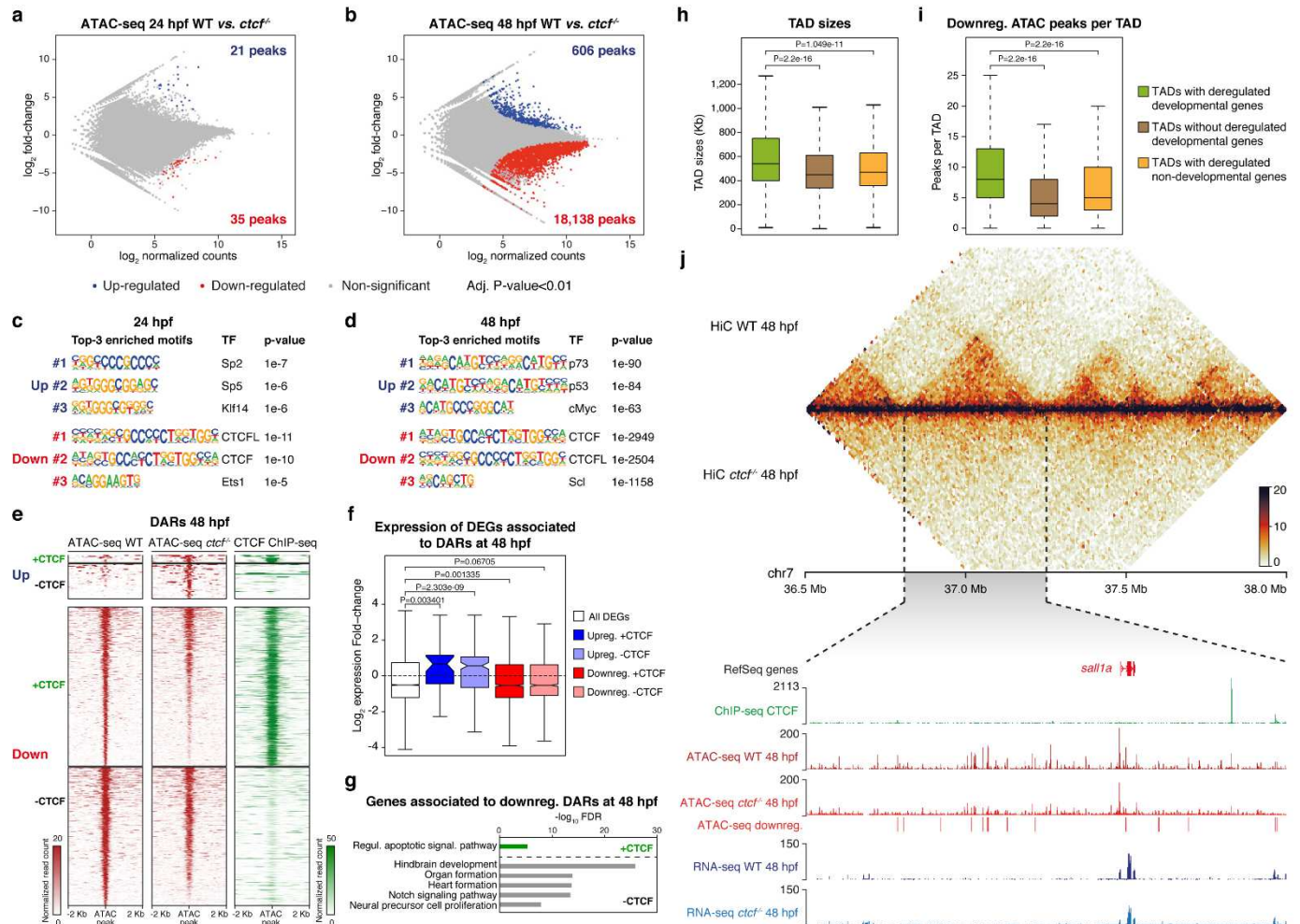
178 **CTCF is required for chromatin accessibility at developmental CREs**

179 The expression of developmental genes is often regulated by multiple tissue-specific CREs,
 180 on which combinations of transcription factors (TFs) are bound, giving rise to precise spatial
 181 and temporal expression patterns. Since CTCF absence affects the expression of
 182 developmental genes mostly without binding to their promoters, we reasoned that this could
 183 be due to alterations in the function of their associated CREs. To test this, we performed ATAC-
 184 seq in wild-type and *ctcf*^{-/-} embryos at 24 and 48 hpf. At 24 hpf, we only found 56 differentially

185 accessible regions (DARs), 21 with increased (up-regulated) and 35 with decreased
186 accessibility (down-regulated) (Fig. 3a). However, at 48 hpf we found a total of 18,744 DARs,
187 most of them down-regulated (18,138 sites vs. 606 up-regulated) (Fig. 3b), temporally
188 coinciding with the detected altered expression of developmental genes (Fig. 2b). Indeed,
189 when we analyzed CREs gaining or losing accessibility in wild-type embryos from 24 to 48 hpf,
190 we found that these sites failed to gain or lose accessibility in *ctcf*^{-/-} embryos (Supplementary
191 Fig. 5), indicating that loss of CTCF impacts chromatin accessibility of thousands of CREs.
192 Motif enrichment analysis showed that the CTCF consensus binding sequence was specifically
193 enriched in down-regulated peaks, both at 24 and 48 hpf (Fig. 3c-d). We confirmed this by
194 analyzing CTCF binding to DARs at 48 hpf and found that 17.5% of up-regulated but 53.5% of
195 down-regulated peaks were bound by CTCF (Fig. 3e). In contrast, up-regulated peaks were
196 enriched for the p53 family motif at 48 hpf. At this stage we also found increased expression
197 of *tp53* and well-known p53 target genes (Fig. 3d; Supplementary Fig. 6), pointing towards an
198 increased apoptotic response in *ctcf*^{-/-} mutants¹⁴. To test a possible contribution of p53 to the
199 mutant phenotypes, we injected one-cell stage embryos with a morpholino to knock-down *tp53*
200 expression. Despite reduced p53-target gene expression and loss of p53-target motif in
201 morpholino-injected mutants, differential accessibility remained unaffected (Supplementary
202 Fig. 6). Furthermore, the p53 knockdown did not change the mutant phenotype at 48 hpf,
203 indicating that the phenotypic response may not be driven by pro-apoptotic processes.

204 Next, we associated DARs to nearby DEGs and found that the average change in gene
205 expression was consistent with the tendency of changes in chromatin accessibility and
206 independent of CTCF binding (Fig. 3f). Interestingly, only down-regulated peaks without CTCF
207 binding were associated with genes enriched in developmental functions, such as hindbrain
208 development or heart formation (Fig. 3g). This indicates that loss of CTCF affects indirectly the
209 accessibility of developmental CREs. We also noted that down-regulated ATAC peaks without
210 CTCF binding sites were highly clustered within the regulatory landscapes of developmental
211 genes, many of them strongly down-regulated in the mutant (Supplementary Fig. 7a-c). This
212 is consistent with the view that developmental genes frequently locate within large gene
213 deserts containing many CREs. Indeed, we found that TADs containing miss-regulated
214 developmental genes were larger and had more associated CREs than those containing non-
215 developmental genes (Fig. 3h-i). Several examples illustrate this tendency. The *sall1a* gene,
216 encoding a transcriptional repressor involved in organogenesis, is in a TAD whose structure
217 was lost in *ctcf*^{-/-} embryos (Fig. 3j). The expression of *sall1a* was reduced in the absence of
218 CTCF and several CREs exhibited reduced accessibility with most of them not binding CTCF.
219 Other examples included the *lhx1a* and *sox11b* genes, both encoding developmental

220 transcription factors (Supplementary Fig. 7d-e). Altogether, these data show that CTCF is
 221 required for the accessibility of thousands of CREs, many of which are associated with
 222 developmental genes.
 223



225 **Figure 3. CTCF promotes chromatin accessibility at developmental cis-regulatory elements.** a-b, Differential
 226 analyses of chromatin accessibility between WT and *ctcf*^{-/-} embryos at 24 (a) and 48 hpf (b) from ATAC-seq data
 227 (n = 2 biological replicates per condition). The log₂ normalized read counts of WT ATAC peaks versus the log₂
 228 fold-change of accessibility are plotted. Regions showing a statistically significant differential accessibility (adjusted P-
 229 value < 0.01) are highlighted in blue (up-regulated) or red (down-regulated). The number of peaks that correspond
 230 to the up- and down-regulated sites are shown inside the boxes. c-d, Motif enrichment analyses for the up- and
 231 down-regulated ATAC peaks in *ctcf*^{-/-} embryos at 24 (c) and 48 hpf (d). The 3 motifs with the lowest p-values are
 232 shown for each case. e, Heatmaps plotting normalized ATAC-seq signal in WT and *ctcf*^{-/-} embryos at 48 hpf (red),
 233 as well as CTCF ChIP-seq signal (green), for the differentially accessible regions (DARs) from (b) overlapping or
 234 not with CTCF peaks. f, Box plots showing the expression fold-change in *ctcf*^{-/-} embryos at 48 hpf of all DEGs or
 235 only those associated with up-regulated or down-regulated DARs, overlapping or not with CTCF sites. Center line,
 236 median; box limits, upper and lower quartiles; whiskers, 1.5x interquartile range; notches, 95% confidence interval
 237 of the median. Statistical significance was assessed using the Wilcoxon's rank sum test. g, GO enrichment analyses
 238 of biological processes for the genes associated with down-regulated DARs in *ctcf*^{-/-} embryos at 48 hpf, overlapping
 239 or not with CTCF sites. GO terms showing an FDR < 0.05 are considered as enriched. h-i, Box plots showing the
 240 TAD sizes (h) and the number of down-regulated DARs per TAD (i) for TADs containing developmental miss-
 241 regulated genes, TADs not containing developmental miss-regulated genes and TADs containing only non-
 242 developmental miss-regulated genes. Center line, median; box limits, upper and lower quartiles; whiskers, 1.5x
 243 interquartile range. Statistical significance was assessed using the Wilcoxon's rank sum test. j, Top, heatmaps
 244 showing HiC signal in WT and *ctcf*^{-/-} embryos at 48 hpf in a 1.5-Mb region of chromosome 7. Bottom, zoom within
 245 the *sall1a* TAD showing UCSC Genome Browser tracks with CTCF ChIP-seq, ATAC-seq at 48 hpf in WT and *ctcf*^{-/-}

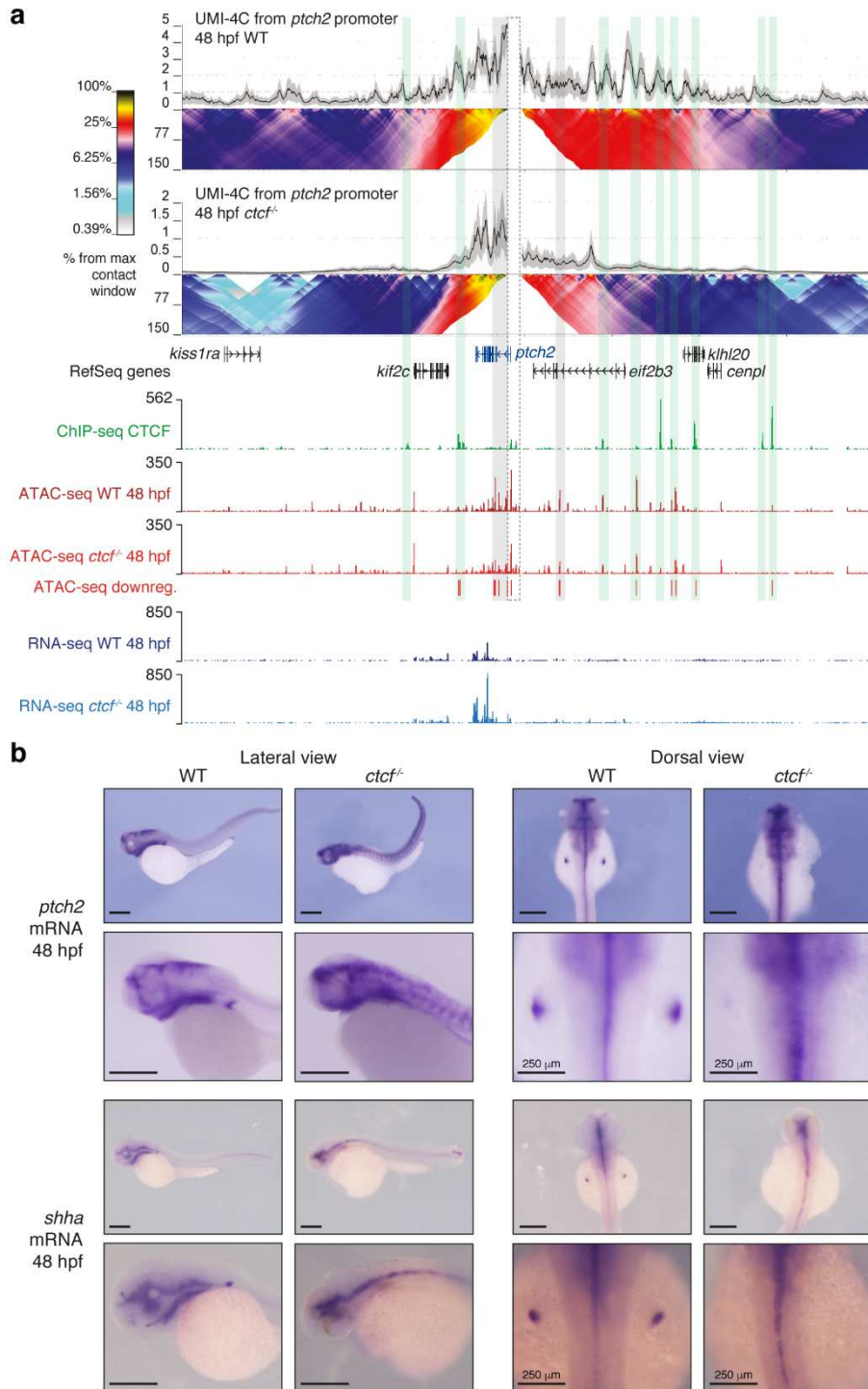
246 ^{-/-} embryos, ATAC-seq down-regulated peaks and RNA-seq at 48 hpf in WT and *ctcf*^{-/-} embryos. The *sal1a* gene is
247 shown in red because it is down-regulated.
248

249 **CTCF is required for the spatiotemporal expression patterns of developmental genes**

250 We have shown so far that CTCF is not only required for chromosome folding during zebrafish
251 development, but also for the robust expression levels of many developmental genes and
252 chromatin accessibility at their regulatory landscapes. To better assess gene miss-expression
253 in relation to the loss of chromatin structure, we first investigated chromatin interactions at the
254 enhancer-promoter level with high resolution by performing UMI-4C experiments. We used
255 developmental gene promoters as viewpoints to analyze their regulatory landscapes in wild-
256 type and *ctcf*^{-/-} embryos at 48 hpf, such as the *ptch2* promoter. *Ptch2* is a patterning gene that
257 encodes a cell receptor binding the Shh morphogen and whose expression was detected as
258 up-regulated by RNA-seq in *ctcf*^{-/-} mutants (Fig. 4a). We found that contacts from the *ptch2*
259 promoter spanned a region of about 500 kb in wild-type embryos, establishing contacts with
260 many genomic regions that included ATAC peaks (potential CREs) with and without CTCF
261 binding (Fig. 4a). However, the *ptch2* regulatory landscape was drastically reduced in *ctcf*^{-/-}
262 embryos. The interaction profile was generally characterized by a loss of long-range contacts
263 but retaining some contacts at shorter ranges (Fig. 4a), consistent with observations in
264 mammalian cells^{32,46}. Genomic regions showing a reduced contact frequency with the *ptch2*
265 promoter included CTCF-binding sites as well as ATAC peaks not bound by CTCF. While some
266 of those peaks losing contacts showed reduced accessibility in the mutant, others were not
267 affected by CTCF absence, suggesting that the decreased enhancer-promoter interactions do
268 not occur as a consequence of decreased TF binding. These results indicate that enhancer-
269 promoter contacts were severely affected by the absence of CTCF, and in particular, long-
270 range interactions.

271 Next, we investigated whether this loss of contacts altered the expression pattern of
272 *ptch2* by performing whole-embryo *in situ* hybridization. *Ptch2* mRNA was detected in the
273 brain, pharyngeal arches and pectoral fin buds of wild-type embryos, but we found that this
274 pattern was severely altered in *ctcf*^{-/-} embryos (Fig. 4b). Consistent with the upregulation in our
275 bulk RNA-seq data, *ptch2* expression in mutant embryos was extended to broader regions of
276 the brain, pharyngeal arches, neural tube and a prominent expansion of expression was
277 observed in the somites. The expression of *ptch2* in the pectoral fin buds was not detected
278 likely due to the severely impaired development at this developmental stage (Fig. 4b),
279 corroborating previous results in *ctcf*-deficient mouse limb buds³⁹. *Ptch2* is expressed in
280 several Shh-responsive tissues and its upregulation in multiple tissues suggested an elevated
281 Shh pathway activity⁴⁷. We therefore looked at the expression pattern of *shha* in wild-type

282 embryos and detected overlapping expression domains with *ptch2* in the brain, the floor plate
283 of the neural tube, the pharyngeal arches and the pectoral fin buds. In *ctcf*^{-/-} embryos, *shha*
284 expression domains were differently affected, with reduced expression in the branchial arches
285 and similar wild-type expression in the brain and the floor plate, which contrasts with the
286 elevated expression of its receptor, *ptch2*, in those domains (Fig. 4b). Altogether, these results
287 suggest that increased *ptch2* expression is not due to increased Shh signaling and that CTCF
288 loss disrupts developmental gene regulatory circuits likely due to the impairment of chromatin
289 structure and enhancer-promoter interactions. Similar changes in the chromatin interactions of
290 regulatory landscapes and gene expression patterns were observed at the HoxD cluster.
291 Viewpoints from the promoters of *hoxd4a* and *hoxd13a* showed reduced interactions within
292 their regulatory landscapes in *ctcf*^{-/-} embryos, especially long-range contacts ([Supplementary](#)
293 [Fig. 8a](#)). Although we could not detect mis-regulation of *hoxd4a* and *hoxd13a* by RNA-seq, *in*
294 *situ* hybridization experiments showed a clear reduction of their expression levels
295 ([Supplementary Fig. 8b](#)). However, other *hox* genes showed consistent mis-regulation
296 detected by both techniques ([Supplementary Fig. 8c](#)). Altogether, our data indicate that CTCF
297 is required to establish chromatin contacts of gene promoters with their associated regulatory
298 landscape and to ensure the accurate spatiotemporal expression patterns of developmental
299 genes.



300

301 **Figure 4. CTCF is required to sustain the regulatory landscapes and complex expression patterns of**
 302 **developmental genes. a**, Top, UMI-4C assays in WT and *ctcf*^{-/-} embryos at 48 hpf using the *ptch2* gene promoter
 303 as a viewpoint. Black lines and grey shadows represent the average normalized UMI counts and their standard
 304 deviation, respectively. Domainograms below UMI counts represent contact frequency between pairs of genomic
 305 regions. Bottom, UCSC Genome Browser tracks with CTCF ChIP-seq, ATAC-seq at 48 hpf in WT and *ctcf*^{-/-}
 306 embryos, ATAC-seq down-regulated peaks and RNA-seq at 48 hpf in WT and *ctcf*^{-/-} embryos. The *ptch2* gene is
 307 shown in blue because it is up-regulated. A dotted-line square represents the restriction fragment containing the
 308 *ptch2* gene promoter that is used as a viewpoint; green shadows highlight CTCF sites and grey shadows highlight
 309 down-regulated ATAC-peaks without CTCF binding. **b**, Whole-mount *in situ* hybridization of the *ptch2* and *shha*
 310 genes in WT and *ctcf*^{-/-} embryos at 48 hpf. Left, lateral view; right, dorsal view. Scale bars represent 500 μ m,
 311 unless indicated.

312

313 Discussion

314 In this work, we have established a new *in vivo* model to study the loss of CTCF in zebrafish
315 and demonstrate that chromatin structure is required to maintain developmental gene
316 regulatory landscapes during body plan formation. In the last years, the function of CTCF in
317 chromosome folding has been clearly demonstrated in mammalian *in vitro* systems, including
318 mouse embryonic stem cells, neural progenitor cells as well as human morula embryos^{5,15,32}.
319 These studies showed by different depletion mechanisms that CTCF knock-down severely
320 reduces TAD formation and insulation. Accordingly, we show here that CTCF is also required
321 for chromatin structure in zebrafish embryos (Fig. 1), extending these conclusions to
322 vertebrates and in agreement with a recent report showing that CTCF knockdown in *Xenopus*
323 embryos altered chromatin structure⁴³.

324 Despite this well-known function of CTCF, its requirement for the regulation of gene
325 expression has remained controversial. The studies mentioned above showed modest effects
326 of CTCF depletion in gene expression, suggesting that steady-state transcription is mostly
327 resistant to genome-wide alteration of chromatin structure. This contrasts with the observation
328 that CTCF is essential for embryonic development¹⁴, but suggests that CTCF-mediated
329 chromatin structure could be essential for processes in which cells respond to multiple signals
330 and where transcriptional control is highly dynamic. However, the early embryonic lethality of
331 CTCF knockout in animal models, has impeded the analysis of CTCF function for
332 transcriptional regulation beyond pluripotency and during the setting up of the animal body
333 plan. Our *ctcf* mutant zebrafish model overcomes this limitation due to the prolonged maternal
334 contribution that lasts, at least, until gastrulation. This allows *ctcf*^{-/-} embryos to develop until
335 stages in which patterning and organogenesis take place. Using this model, we observe for
336 the first time in developing embryos the miss-regulation of thousands of genes (Fig. 2), among
337 which many lineage-specific genes that are dynamically regulated during development. These
338 observations are consistent with recent reports, showing that CTCF is required for the
339 expression of a subset of lineage-specific genes during cell differentiation³² and for fast
340 transcriptional responses to external stimuli⁴⁸.

341 The expression of developmental genes is characterized by a tight spatiotemporal
342 control by CREs that constitute their regulatory landscapes. These have been shown to largely
343 coincide with TADs and to be constrained by TAD boundaries⁴⁹. Here, we show that chromatin
344 accessibility at CTCF sites but also at thousands of CREs is compromised in *ctcf* mutants (Fig.
345 3). Specifically, clusters of CREs within large TADs of developmental genes show highly
346 reduced accessibility, most of them without direct CTCF binding. This suggests reduced TF
347 binding at CREs that may arise either due to their decreased expression levels or decreased

348 enhancer-promoter interactions. Miss-expression of TFs during development likely induces
349 changes in downstream target gene expression that may contribute to the observed global
350 gene miss-expression. To distinguish between TF-induced effects and effects induced by
351 changes in chromatin structure, we analyzed several developmental loci in detail. High-
352 resolution analyses of the *ptch2*, *hoxd4a* and *hoxd13a* gene regulatory landscapes show that
353 many CREs lose contacts with their promoters in the absence of CTCF. These are primarily
354 long-range contacts but without a clear bias for only CREs that are differentially regulated (Fig.
355 4 and Supplementary Fig. 8), suggesting that CTCF-mediated chromatin structure at these loci
356 is required for CRE-promoter contacts independently of TF availability at CREs. This is in
357 agreement with recent observations showing that CTCF is required for long-range enhancer-
358 promoter contacts^{32,46}. While it is unlikely that CTCF directly mediates those enhancer-
359 promoter interactions, it may favor their establishment by promoting contacts within the
360 involved TADs. It has been shown previously that the loss of CTCF binding sites that contribute
361 to the general TAD structure of a locus are required for CRE-promoter interactions to ensure
362 robust gene expression during development³⁵⁻³⁷. In addition to the reduced contacts within
363 those regulatory landscapes, we show here that the complex expression patterns of these
364 genes are altered in a tissue-specific manner, showing up- and down-regulation in different
365 embryonic domains (Fig. 4). This is illustrated by the functionally connected genes *ptch2* and
366 *shha*. While under normal conditions the expression of both gene co-depends, their different
367 expression patterns in several embryonic domains in *ctcf*^{-/-} mutants suggests that the absence
368 of CTCF leads to their functional disconnection and gene miss-expression as consequence of
369 an altered chromatin structure at their respective regulatory landscapes.

370 In summary, our data demonstrate that CTCF is essential to sustain large regulatory
371 landscapes of developmental genes during embryonic development. This would favor the
372 proper interaction of multiple CREs with their target genes, leading to the complex
373 spatiotemporal expression patterns of developmental genes. It has been suggested that TADs
374 may have evolved as conserved scaffolds for developmental gene regulatory landscapes⁵⁰.
375 Our observations support this view by linking chromatin structure at regulatory landscapes with
376 gene function.

377

378 References

- 379 1 Bell, A. C., West, A. G. & Felsenfeld, G. The protein CTCF is required for the
380 enhancer blocking activity of vertebrate insulators. *Cell* **98**, 387-396,
381 doi:10.1016/s0092-8674(00)81967-4 (1999).
- 382 2 Filippova, G. N. *et al.* An exceptionally conserved transcriptional repressor, CTCF,
383 employs different combinations of zinc fingers to bind diverged promoter sequences

384 of avian and mammalian c-myc oncogenes. *Mol Cell Biol* **16**, 2802-2813,
385 doi:10.1128/mcb.16.6.2802 (1996).

386 3 Merkschlager, M. & Nora, E. P. CTCF and Cohesin in Genome Folding and
387 Transcriptional Gene Regulation. *Annu Rev Genomics Hum Genet* **17**, 17-43,
388 doi:10.1146/annurev-genom-083115-022339 (2016).

389 4 Phillips, J. E. & Corces, V. G. CTCF: master weaver of the genome. *Cell* **137**, 1194-
390 1211, doi:10.1016/j.cell.2009.06.001 (2009).

391 5 Nora, E. P. *et al.* Targeted Degradation of CTCF Decouples Local Insulation of
392 Chromosome Domains from Genomic Compartmentalization. *Cell* **169**, 930-944
393 e922, doi:10.1016/j.cell.2017.05.004 (2017).

394 6 Dixon, J. R. *et al.* Topological domains in mammalian genomes identified by analysis
395 of chromatin interactions. *Nature* **485**, 376-380, doi:10.1038/nature11082 (2012).

396 7 Hou, C., Li, L., Qin, Z. S. & Corces, V. G. Gene density, transcription, and insulators
397 contribute to the partition of the Drosophila genome into physical domains. *Mol Cell*
398 **48**, 471-484, doi:10.1016/j.molcel.2012.08.031 (2012).

399 8 Nora, E. P. *et al.* Spatial partitioning of the regulatory landscape of the X-inactivation
400 centre. *Nature* **485**, 381-385, doi:10.1038/nature11049 (2012).

401 9 Sexton, T. *et al.* Three-dimensional folding and functional organization principles of
402 the Drosophila genome. *Cell* **148**, 458-472, doi:10.1016/j.cell.2012.01.010 (2012).

403 10 Rao, S. S. *et al.* A 3D map of the human genome at kilobase resolution reveals
404 principles of chromatin looping. *Cell* **159**, 1665-1680, doi:10.1016/j.cell.2014.11.021
405 (2014).

406 11 Splinter, E. *et al.* CTCF mediates long-range chromatin looping and local histone
407 modification in the beta-globin locus. *Genes Dev* **20**, 2349-2354,
408 doi:10.1101/gad.399506 (2006).

409 12 Phillips-Cremins, J. E. *et al.* Architectural protein subclasses shape 3D organization
410 of genomes during lineage commitment. *Cell* **153**, 1281-1295,
411 doi:10.1016/j.cell.2013.04.053 (2013).

412 13 Heath, H. *et al.* CTCF regulates cell cycle progression of alphabeta T cells in the
413 thymus. *EMBO J* **27**, 2839-2850, doi:10.1038/emboj.2008.214 (2008).

414 14 Moore, J. M. *et al.* Loss of maternal CTCF is associated with peri-implantation
415 lethality of Ctcf null embryos. *PLoS One* **7**, e34915,
416 doi:10.1371/journal.pone.0034915 (2012).

417 15 Chen, X. *et al.* Key role for CTCF in establishing chromatin structure in human
418 embryos. *Nature* **576**, 306-310, doi:10.1038/s41586-019-1812-0 (2019).

419 16 de Laat, W. & Duboule, D. Topology of mammalian developmental enhancers and
420 their regulatory landscapes. *Nature* **502**, 499-506, doi:10.1038/nature12753 (2013).

421 17 Furlong, E. E. M. & Levine, M. Developmental enhancers and chromosome topology.
422 *Science* **361**, 1341-1345, doi:10.1126/science.aau0320 (2018).

423 18 Franke, M. & Gomez-Skarmeta, J. L. An evolutionary perspective of regulatory
424 landscape dynamics in development and disease. *Curr Opin Cell Biol* **55**, 24-29,
425 doi:10.1016/j.ceb.2018.06.009 (2018).

426 19 Bonev, B. & Cavalli, G. Organization and function of the 3D genome. *Nat Rev Genet*
427 **17**, 661-678, doi:10.1038/nrg.2016.112 (2016).

428 20 Dekker, J. & Mirny, L. The 3D Genome as Moderator of Chromosomal
429 Communication. *Cell* **164**, 1110-1121, doi:10.1016/j.cell.2016.02.007 (2016).

430 21 Dixon, J. R., Gorkin, D. U. & Ren, B. Chromatin Domains: The Unit of Chromosome
431 Organization. *Mol Cell* **62**, 668-680, doi:10.1016/j.molcel.2016.05.018 (2016).

432 22 McCord, R. P., Kaplan, N. & Giorgetti, L. Chromosome Conformation Capture and
433 Beyond: Toward an Integrative View of Chromosome Structure and Function. *Mol*
434 *Cell* **77**, 688-708, doi:10.1016/j.molcel.2019.12.021 (2020).

435 23 Rowley, M. J. & Corces, V. G. Organizational principles of 3D genome architecture.
436 *Nat Rev Genet* **19**, 789-800, doi:10.1038/s41576-018-0060-8 (2018).

437 24 Fudenberg, G. *et al.* Formation of Chromosomal Domains by Loop Extrusion. *Cell Rep* **15**, 2038-2049, doi:10.1016/j.celrep.2016.04.085 (2016).

438

439 25 Sanborn, A. L. *et al.* Chromatin extrusion explains key features of loop and domain
440 formation in wild-type and engineered genomes. *Proc Natl Acad Sci U S A* **112**,
441 E6456-6465, doi:10.1073/pnas.1518552112 (2015).

442 26 Rao, S. S. P. *et al.* Cohesin Loss Eliminates All Loop Domains. *Cell* **171**, 305-320
443 e324, doi:10.1016/j.cell.2017.09.026 (2017).

444 27 Franke, M. *et al.* Formation of new chromatin domains determines pathogenicity of
445 genomic duplications. *Nature* **538**, 265-269, doi:10.1038/nature19800 (2016).

446 28 Laugsch, M. *et al.* Modeling the Pathological Long-Range Regulatory Effects of
447 Human Structural Variation with Patient-Specific hiPSCs. *Cell Stem Cell* **24**, 736-752
448 e712, doi:10.1016/j.stem.2019.03.004 (2019).

449 29 Lupianez, D. G. *et al.* Disruptions of topological chromatin domains cause pathogenic
450 rewiring of gene-enhancer interactions. *Cell* **161**, 1012-1025,
451 doi:10.1016/j.cell.2015.04.004 (2015).

452 30 Spielmann, M., Lupianez, D. G. & Mundlos, S. Structural variation in the 3D genome.
453 *Nat Rev Genet* **19**, 453-467, doi:10.1038/s41576-018-0007-0 (2018).

454 31 Symmons, O. *et al.* The Shh Topological Domain Facilitates the Action of Remote
455 Enhancers by Reducing the Effects of Genomic Distances. *Dev Cell* **39**, 529-543,
456 doi:10.1016/j.devcel.2016.10.015 (2016).

457 32 Kubo, N. *et al.* CTCF Promotes Long-range Enhancer-promoter Interactions and
458 Lineage-specific Gene Expression in Mammalian Cells. *bioRxiv*,
459 2020.2003.2021.001693, doi:10.1101/2020.03.21.001693 (2020).

460 33 Ghavi-Helm, Y. *et al.* Highly rearranged chromosomes reveal uncoupling between
461 genome topology and gene expression. *Nat Genet* **51**, 1272-1282,
462 doi:10.1038/s41588-019-0462-3 (2019).

463 34 Williamson, I. *et al.* Developmentally regulated Shh expression is robust to TAD
464 perturbations. *Development* **146**, doi:10.1242/dev.179523 (2019).

465 35 Despang, A. *et al.* Functional dissection of the Sox9-Kcnj2 locus identifies
466 nonessential and instructive roles of TAD architecture. *Nat Genet* **51**, 1263-1271,
467 doi:10.1038/s41588-019-0466-z (2019).

468 36 Hnisz, D. *et al.* Activation of proto-oncogenes by disruption of chromosome
469 neighborhoods. *Science* **351**, 1454-1458, doi:10.1126/science.aad9024 (2016).

470 37 Paliou, C. *et al.* Preformed chromatin topology assists transcriptional robustness of
471 Shh during limb development. *Proc Natl Acad Sci U S A* **116**, 12390-12399,
472 doi:10.1073/pnas.1900672116 (2019).

473 38 Gomez-Velazquez, M. *et al.* CTCF counter-regulates cardiomyocyte development
474 and maturation programs in the embryonic heart. *PLoS Genet* **13**, e1006985,
475 doi:10.1371/journal.pgen.1006985 (2017).

476 39 Soshnikova, N., Montavon, T., Leleu, M., Galjart, N. & Duboule, D. Functional
477 analysis of CTCF during mammalian limb development. *Dev Cell* **19**, 819-830,
478 doi:10.1016/j.devcel.2010.11.009 (2010).

479 40 Vejnar, C. E. *et al.* Genome wide analysis of 3' UTR sequence elements and proteins
480 regulating mRNA stability during maternal-to-zygotic transition in zebrafish. *Genome*
481 *Res* **29**, 1100-1114, doi:10.1101/gr.245159.118 (2019).

482 41 Kaaij, L. J. T., van der Weide, R. H., Ketting, R. F. & de Wit, E. Systemic Loss and
483 Gain of Chromatin Architecture throughout Zebrafish Development. *Cell Rep* **24**, 1-10
484 e14, doi:10.1016/j.celrep.2018.06.003 (2018).

485 42 Crane, E. *et al.* Condensin-driven remodelling of X chromosome topology during
486 dosage compensation. *Nature* **523**, 240-244, doi:10.1038/nature14450 (2015).

487 43 Niu, L. *et al.* Systematic Chromatin Architecture Analysis in *Xenopus*
488 *tropicalis* Reveals Conserved Three-Dimensional Folding Principles of

489 Vertebrate Genomes. *bioRxiv*, 2020.2004.2002.021378,
490 doi:10.1101/2020.04.02.021378 (2020).
491 44 de Wit, E. *et al.* CTCF Binding Polarity Determines Chromatin Looping. *Mol Cell* **60**,
492 676-684, doi:10.1016/j.molcel.2015.09.023 (2015).
493 45 Gomez-Marin, C. *et al.* Evolutionary comparison reveals that diverging CTCF sites
494 are signatures of ancestral topological associating domains borders. *Proc Natl Acad*
495 *Sci U S A* **112**, 7542-7547, doi:10.1073/pnas.1505463112 (2015).
496 46 Thiecke, M. J. *et al.* Cohesin-Dependent and -Independent Mechanisms Mediate
497 Chromosomal Contacts between Promoters and Enhancers. *Cell Rep* **32**, 107929,
498 doi:10.1016/j.celrep.2020.107929 (2020).
499 47 Briscoe, J., Chen, Y., Jessell, T. M. & Struhl, G. A hedgehog-insensitive form of
500 patched provides evidence for direct long-range morphogen activity of sonic
501 hedgehog in the neural tube. *Mol Cell* **7**, 1279-1291, doi:10.1016/s1097-
502 2765(01)00271-4 (2001).
503 48 Stik, G. *et al.* CTCF is dispensable for immune cell transdifferentiation but facilitates
504 an acute inflammatory response. *Nat Genet*, doi:10.1038/s41588-020-0643-0 (2020).
505 49 Harmston, N. *et al.* Topologically associating domains are ancient features that
506 coincide with Metazoan clusters of extreme noncoding conservation. *Nat Commun* **8**,
507 441, doi:10.1038/s41467-017-00524-5 (2017).
508 50 Acemel, R. D., Maeso, I. & Gomez-Skarmeta, J. L. Topologically associated domains:
509 a successful scaffold for the evolution of gene regulation in animals. *Wiley Interdiscip*
510 *Rev Dev Biol* **6**, doi:10.1002/wdev.265 (2017).
511

512 **Methods**

513

514 **Animal experimentation**

515 Wild-type AB/Tübingen zebrafish strains were maintained and bred under standard conditions.
516 All experiments involving animals conform national and European Community standards for
517 the use of animals in experimentation and were approved by the Ethical Committees from the
518 University Pablo de Olavide, CSIC and the Andalusian government.

519

520 **CRISPR-Cas9 genome editing**

521 CRISPR target sites to mutate the *ctcf* gene were identified using the CRISPRscan online
522 tool⁵¹. Two single guide RNAs (sgRNAs) targeting the exons 4 and 5 of the *ctcf* gene were
523 used with the following target sequences: 5'-GGA GTT ACA CTT GCC CAC GC-3' and 5'-
524 GGC ATG GCC TTT GTC ACC AG-3'. The template DNA for sgRNA transcription was
525 generated by PCR using CTCFexon4, CTCFexon5 and sgRNA_universal primers
526 ([Supplementary Table 1](#)) and Phusion DNA polymerase (Thermo Fisher Scientific). sgRNAs
527 were *in vitro* transcribed using the HiScribe T7 Quick High Yield RNA synthesis kit (NEB) using
528 75 ng of template, treated with DNase I (NEB) and purified using the RNA Clean and
529 Concentrator kit (Zymo Research).

530 One-cell stage zebrafish embryos were injected with 2-3 nl of a solution containing 140
531 ng/ μ l of Cas9 mRNA and 25 ng/ μ l of each sgRNA. The CRISPR-Cas9 approach generated a
532 deletion of 260 bp encompassing exons 4 and 5 and resulting in a premature STOP codon in
533 exon 5. The predicted truncated protein had 343 amino acids instead of 798, lacking ten and
534 a half of the eleven zinc finger domains of the CTCF protein. For genotyping, genomic DNA
535 was obtained by incubating the samples (whole embryos or adult caudal fin fragments) in TE
536 buffer supplemented with 5% Chelex-100 (BioRad) and 10 μ g/ml Proteinase K (Roche) for 1h
537 (embryos) or 4h (fins) at 55°C and 10 min at 95°C, and then stored at 4°C. One microliter of
538 the supernatant was used as a template for standard 20 μ l PCR reactions using CTCFpF and
539 CTCFpR primers ([Supplementary Table 1](#)), resulting in 842- or 582-bp amplicons for wild type
540 or mutant alleles, respectively. The mutant allele was stably maintained in heterozygosis with
541 no apparent phenotypes but homozygous mutants are embryonic lethal (<3 days).

542

543 **Whole-mount embryo immunofluorescence**

544 For immunofluorescence, embryos were fixed overnight at 4°C with 4% paraformaldehyde,
545 washed in PBT (PBS supplemented with 0.2% Triton-X100) and blocked in this solution with
546 2% goat serum and 2 mg/ml BSA for 1 h at RT. Then, they were incubated overnight at 4°C

547 with primary antibody specific for zebrafish CTCF⁵² (used in 1:500 dilution). After extensive
548 washings with PBT, embryos were incubated overnight at 4°C with goat anti-rabbit Alexa Fluor
549 488 secondary antibody (used 1:800 dilution, A27034 Invitrogen). Finally, embryos were flat-
550 mounted and imaged under an SP confocal microscope (Leica).

551

552 **Whole-mount embryo *in situ* hybridization**

553 Antisense RNA probes were prepared from cDNA using digoxigenin (Boehringer Mannheim)
554 as label and the primers listed in [Supplementary Table 1](#), except those for *shha* and *hoxd13a*
555 that were previously described⁵³. Zebrafish embryos were prepared, hybridized and stained
556 using standard protocols⁵⁴. Embryos at 48 hpf stage were fixed in 4% paraformaldehyde
557 overnight, dehydrated in methanol and stored at -20°C. All solutions and reagents used were
558 RNase-free. The embryos were hydrated using decreasing amounts of methanol and finally in
559 PBS-0.1% Tween. Then, they were treated with 10 µg/ml proteinase K for 10 min at room
560 temperature and gently washed with PBS-0.1% Tween. In the pre-hybridization step, embryos
561 were kept at 70°C in the hybridization buffer for at least 1 hour. Then, the probe was diluted to
562 2 ng/µl in hybridization buffer and incubated overnight at 70°C while moving. Pre-heated
563 buffers with decreasing amounts of hybridization buffer (75%, 50%, 25% and 0%) in 2x SSC
564 solution were used to wash embryos for 10 min, plus a 30 min wash at 70°C with 0.05x SSC.
565 Then, they were incubated with Blocking Buffer (PBS-0.1% Tween, 2% normal goat serum, 2
566 mg/ml bovine serum albumin [BSA]) for 1 hour, and with an anti-digoxigenin antibody (1:5,000
567 in Blocking Buffer) for at least 2 hours at room temperature. After this, embryos were washed
568 six times with PBS-0.1% Tween at room temperature and then overnight at 4°C. Next day,
569 embryos were washed once more with PBS-0.1% Tween and three times with fresh AP buffer
570 (100 mM Tris-HCl pH 9.5, 50mM MgCl₂, 100mM NaCl, 0.1% Tween), followed by signal
571 development with NBT/BCIP solution (225 µg/ml NBT, 175 µg/ml BCIP) in multi-well plates in
572 the dark. Signal development was stopped by washing with PBS-0.1% Tween and fixing with
573 4% paraformaldehyde. Imaging of the *in situ* hybridization signal was performed in MZ-12
574 dissecting scope (Leica).

575

576 **RNA-seq**

577 For total RNA extraction, wild-type and *ctcf*^{-/-} single embryos at 24 or 48 hpf were collected,
578 manually de-chorionated and suspended in TRIsure (Bioline) with chloroform. DNA was used
579 for genotyping and single wild-type and *ctcf*^{-/-} individuals were selected for RNA-seq
580 experiments. Precipitated RNA was then treated with TURBO DNA free kit (Invitrogen). Two
581 biological replicates were used for each analyzed genotype and stage.

582 Illumina libraries were constructed and sequenced in a BGISEQ-500 single-end lane
583 producing around 50 million (M) of 50-bp reads. Reads were aligned to the GRCz10
584 (danRer10) zebrafish genome assembly using STAR 2.5.3a⁵⁵ and counted using the htseq-
585 count tool from the HTSeq 0.8.0 toolkit⁵⁶. Differential gene expression analysis was performed
586 using the DESeq2 1.18.1 package in R 3.4.3⁵⁷, setting a corrected P value < 0.01 as the cutoff
587 for statistical significance of the differential expression. Enrichment of GO Biological Process
588 terms was calculated using David⁵⁸, with a false discovery rate (FDR)-corrected P value < 0.05
589 as statistical cutoff.

590

591 **ATAC-seq**

592 ATAC-seq assays were performed using standard protocols^{59,60}, with minor modifications.
593 Briefly, single WT or *ctcf*^{-/-} mutant embryos at 24 or 48 hpf coming from *ctcf*^{+/-} crosses were
594 manually de-chorionated. Yolk was dissolved with Ginzburg Ring Finger (55 mM NaCl, 1.8 mM
595 KCl, 1.15 mM NaHCO₃) by pipetting and shaking 5 min at 1100 rpm. Deyolked embryos were
596 collected by centrifugation for 5 min at 500g 4°C. Supernatant was removed and embryos
597 washed with PBS. Then, embryos were lysed in 50 μ l of Lysis Buffer (10 mM Tris-HCl pH 7.4,
598 10 mM NaCl, 3 mM MgCl₂, 0.1% NP-40, 1x Roche Complete protease inhibitors cocktail) by
599 pipetting up and down. The whole cell lysate was used for TAGmentation, which were
600 centrifuged for 10 min at 500g 4°C and resuspended in 50 μ l of the Transposition Reaction,
601 containing 1.25 μ l of Tn5 enzyme and TAGmentation Buffer (10 mM Tris-HCl pH 8.0, 5 mM
602 MgCl₂, 10 % w/v dimethylformamide), and incubated for 30 min at 37°C. Immediately after
603 TAGmentation, DNA was purified using the Minelute PCR Purification Kit (Qiagen) and eluted
604 in 20 μ l. Before library amplification, purified DNA was used to genotype 24-hpf embryos (see
605 above) and wild-type or *ctcf*^{-/-} mutants were selected for deep sequencing. Libraries were
606 generated by PCR amplification using NEBNext High-Fidelity 2X PCR Master Mix (NEB). The
607 resulting libraries were multiplexed and sequenced in a HiSeq 4000 pair-end lane producing
608 100M of 49-bp pair end reads per sample.

609

610 **ChIPmentation**

611 ChIP-seq of CTCF was performed by ChIPmentation, which incorporates Tn5-mediated
612 TAGmentation of immunoprecipitated DNA, as previously described^{61,62}. Briefly, 100 zebrafish
613 embryos at 24 hpf were dechorionated with 300 μ g/ml pronase, fixed for 10 min in 1%
614 paraformaldehyde (in 200 mM phosphate buffer) at room temperature, quenched for 5 min
615 with 0.125 M glycine, washed in PBS and frozen at -80°C. Fixed embryos were homogenized
616 in 2 ml cell lysis buffer (10 mM Tris-HCl pH 7.5, 10 mM NaCl, 0.3% NP-40, 1x Roche Complete

617 protease inhibitors cocktail) with a Dounce Homogenizer on ice and centrifuged 5 min 2,300g
618 at 4°C. Pelleted nuclei were resuspended in 333 μ l of nuclear lysis buffer (50 mM Tris-HCl pH
619 7.5, 10 mM EDTA, 1% SDS, 1x Roche Complete protease inhibitors cocktail), kept 5 min on
620 ice and diluted with 667 μ l of ChIP dilution buffer (16.7 mM Tris-HCl pH 7.5, 1.2 mM EDTA,
621 167 mM NaCl, 0.01% SDS, 1.1% Triton-X100). Then, chromatin was sonicated in a Covaris
622 M220 sonicator (duty cycle 10%, PIP 75W, 100 cycles/burst, 10 min) and centrifuged 5 min
623 18,000g at 4°C. The recovered supernatant, which contained soluble chromatin, was used for
624 ChIP or frozen at -80°C after checking the size of the sonicated chromatin. Four 250 μ l aliquots
625 of sonicated chromatin were used for each independent ChIP experiment, and each aliquot
626 incubated with 2 μ g of anti-CTCF antibody⁵² and rotated overnight at 4°C. Next day, 20 μ l of
627 protein G Dynabeads (Invitrogen) per aliquot were washed twice with ChIP dilution buffer and
628 resuspended in 50 μ l/aliquot of the same solution. Immunoprecipitated chromatin was then
629 incubated with washed beads for 1 hour rotating at 4°C and washed twice sequentially with
630 wash buffer 1 (20 mM Tris-HCl pH 7.5, 2 mM EDTA, 150 mM NaCl, 1% SDS, 1% Triton-X100),
631 wash buffer 2 (20 mM Tris-HCl pH 7.5, 2 mM EDTA, 500 mM NaCl, 0.1% SDS, 1% Triton-
632 X100), wash buffer 3 (10 mM Tris-HCl pH 7.5, 1 mM EDTA, 250 mM LiCl, 1% NP-40, 1% Na-
633 deoxycholate) and 10 mM Tris-HCl pH 8.0, using a cold magnet (Invitrogen). Then, beads were
634 resuspended in 25 μ l of TAGmentation reaction mix (10 mM Tris-HCl pH 8.0, 5 mM MgCl₂, 10
635 % w/v dimethylformamide), added 1 μ l of Tn5 enzyme and incubated 1 min at 37°C.
636 TAGmentation reaction was put in the cold magnet and the supernatant discarded. Beads were
637 washed twice again with wash buffer 1 and 1x TE and eluted twice for 15 min in 100 μ l of
638 elution buffer (50 mM NaHCO₃ pH 8.8, 1% SDS). The 200 μ l of eluted chromatin per aliquot
639 were then decrosslinked by adding 10 μ l of 4M NaCl and 1 μ l of 10 mg/ml proteinase K and
640 incubating at 65°C for 6 hours. DNA was purified using Minelute PCR Purification Kit (Qiagen),
641 pooling all aliquots in a single column, and eluted in 20 μ l. Library preparation was
642 performed as previously described for ATAC-seq (see above). Libraries were multiplexed and
643 sequenced in a HiSeq 4000 pair-end lane producing around 20M of 49-bp paired-end reads
644 per sample.

645

646 **ChIPmentation and ATAC-seq data analyses**

647 ChIPmentation and ATAC-seq reads were aligned to the GRCz10 (danRer10) zebrafish
648 genome assembly using Bowtie2⁶³ and those pairs separated by more than 2 Kb were
649 removed. For ATAC-seq, the Tn5 cutting site was determined as the position -4 (minus strand)
650 or +5 (plus strand) from each read start, and this position was extended 5 bp in both directions.
651 Conversion of SAM alignment files to BAM was performed using Samtools⁶⁴. Conversion of

652 BAM to BED files, and peak analyses, such as overlaps or merges, were carried out using the
653 Bedtools suite⁶⁵. Conversion of BED to BigWig files was performed using the genomecov tool
654 from Bedtools and the wigToBigWig utility from UCSC⁶⁶. For ATAC-seq, peaks were called
655 using MACS2 algorithm⁶⁷ with an FDR < 0.05 for each replicate and merged in a single pool
656 of peaks that was used to calculate differentially accessible sites with DESeq2 1.18.1 package
657 in R 3.4.3⁵⁷, setting a corrected P value < 0.01 as the cutoff for statistical significance of the
658 differential accessibility. For ChIPmentation, peaks with an FDR < 0.001 were called with
659 MACS2. For visualization purposes, reads were extended 100 bp for ATAC-seq and 300 bp
660 for ChIPmentation. For data comparison, all ATAC-seq experiments used were normalized
661 using reads falling into peaks to counteract differences in background levels between
662 experiments and replicates, as previously described⁶¹.

663 Heatmaps and average profiles of ChIPmentation and ATAC-seq data were generated
664 using computeMatrix, plotHeatmap and plotProfile tools from the Deeptools 2.0 toolkit⁶⁸. TF
665 motif enrichment and peak annotation to genomic features were calculated using the scripts
666 FindMotifsGenome.pl and AnnotatePeaks.pl from Homer software⁶⁹, with standard
667 parameters. For gene assignment to ChIP and ATAC peaks, coordinates were converted to
668 Zv9 (danRer7) genome using the Liftover tool of the UCSC Genome Browser⁶⁶ and assigned
669 to genes using the GREAT tool⁷⁰, with the basal plus extension association rule with standard
670 parameters (5 Kb upstream, 1 Kb downstream, 1 Mb maximum extension). Peak clustering
671 was calculated using the mergeBed tool from Bedtools⁶⁵, considering as clustered those peaks
672 located less than 30 Kb from each other.

673

674 **HiC**

675 HiC library preparation was performed as previously described¹⁰ with minor modifications.
676 Experiments were performed for at least two biological replicates in wild-type and *ctcf*^{-/-} mutant
677 embryos at 48 hpf, using one to three million cells as input material.

678 Embryo fixation and nuclei extraction: Pools of 50 zebrafish embryos were dechorionated with
679 300 μ g/ml pronase, followed by fixation for 10 min in 1% paraformaldehyde (in 200 mM
680 phosphate buffer) at room temperature. The reaction was quenched by adding glycine to a
681 final concentration of 0.125 M and incubation at room temperature for 5 min. Embryos were
682 washed on ice twice with 1x PBS and either snap frozen in liquid nitrogen or processed for
683 nuclei extraction. For nuclei extraction, fixed embryos were homogenized in 2-5 ml freshly
684 prepared lysis buffer (50 mM Tris pH7.5; 150 mM NaCl; 5 mM EDTA; 0.5 % NP-40; 1.15 %
685 Triton X-100; 1x Roche Complete protease inhibitors) with a Dounce Homogenizer on ice.

686 Nuclei were pelleted by centrifugation for 5 min, 750g at 4°C and washed with 1x PBS. Pelleted
687 nuclei were either snap-frozen in liquid nitrogen or further processed.

688 Chromatin digestion: Nuclei pellets were resuspended in 100 μ l 0.5% SDS and incubated for
689 10 min at 62°C, without shaking. 292 μ l water and 50 μ l 10% Triton X-100 were added to each
690 sample, mixed, and incubated for 15 min at 37°C to quench remaining SDS. 50 μ l of 10x
691 restriction enzyme buffer and a total of 400 units of DpnII (NEB, R0543) were added to the
692 sample, mixed and incubated overnight at 37°C with 900 rpm shaking.

693 Biotin fill-in and proximity ligation: Restriction enzyme was heat inactivated. Nuclei were
694 pelleted at 600 g for 10 min at 4°C and resuspended in 445 μ l 1x ice-cold NEB buffer 2. For
695 biotin fill-in reaction, 5 μ l of 10x NEB buffer 2, 1.5 μ l 10 mM (each) dNTP-dATP-mix, 37.5 μ l of
696 0.4 mM biotin-14-dATP and 10 μ l of 5 U/ μ l Klenow (NEB, M0210L) were added and mixed by
697 pipetting. Samples were incubated at 25°C for 4 h and 800 rpm shaking. To ligate restriction
698 fragment ends, 500 μ l of 2x ligation mix (100 μ l of 10x ligation buffer (NEB), 100 μ l of 10%
699 Triton-X-100, 10 μ l of 10 mg/ml BSA, 6.5 μ l of T4 DNA ligase (NEB, M0202L), 283.5 μ l water)
700 were added to each sample and incubated overnight at 16°C and 800 rpm shaking .

701 Cross-link reversal and DNA purification: Nuclei were pelleted by centrifugation for 10 min, 600
702 g at 4°C and sample volume was reduced to a total of 200 μ l. 230 μ l of 10 mM Tris HCL pH
703 7.5, 20 μ l of Proteinase K (10mg/ml) and 50 μ l of 10% SDS were added, mixed by pipetting
704 and incubated 30 min at 55°C. Subsequently, 40 μ l of 4 M NaCl were added and samples were
705 incubated overnight at 65°C with 700 rpm shaking. Next, 5 μ l of RNase A (10 mg/ml) were
706 added, followed by incubation at 37°C for 30 min at 700 rpm. 20 μ l Proteinase K (10 mg/ml)
707 were added to the sample and incubated at 55°C for 1-2 h at 700 rpm. DNA was purified by
708 phenol-chloroform extraction. Following DNA precipitation, dried DNA pellet was reconstituted
709 in 100 μ l 10 mM Tris-HCl pH 7.5.

710 Removing biotin from un-ligated fragments and DNA shearing: 5-7 μ g of HiC library in a total
711 volume of 100 μ l (1x NEB buffer 2.1, 0.025 mM dNTPs, 0.12 U/ μ l T4 DNA polymerase (NEB,
712 M0203) was incubated at 20°C for 4 h to remove biotin from unligated ends. Reaction was
713 stopped by adding EDTA to a final concentration of 10 mM and heat inactivation for 20 min at
714 75°C. DNA was sheared, using Covaris M220 sonicator with the following setup: 130 μ l sample
715 volume, Peak Incident Power (W): 50, Duty Factor: 20%, Cycles per Burst: 200, Treatment
716 Time (s): 65, cooling at 7°C. Samples were subsequently size selected for fragments between
717 150 and 600 bp using AMPure XP beads (Agencourt, A63881) as follows: 0.575x volume of
718 AMPure beads were added to the sample, mixed by pipetting, and incubated for 10 min at
719 room temperature. Beads were separated on a magnet, and clear supernatant was transferred
720 to a fresh tube. 0.395x volume of fresh AMPure beads were added to the supernatant, mixed,

721 and incubated for 10 min at room temperature. Beads were separated on a magnet, and clear
722 supernatant was discarded. Beads were washed twice with 70% EtOH, air dried for 5 min and
723 DNA was eluted in 300 μ l water.

724 Biotin pull down: Biotin-labelled DNA was bound to Dynabeads My One C1 Streptavidin beads,
725 using 5 μ l of beads per 1 μ g DNA and following manufacturer's instructions. Beads were
726 washed twice with 1x tween-washing-buffer (5 mM Tris HCl pH 7.5, 0.5 mM EDTA, 1 M NaCl,
727 0.05% Tween 20) and finally resuspended in 1x sample volume 2x binding buffer (10 mM Tris
728 HCl pH 7.5, 1 mM EDTA, 2 M NaCl). Beads were mixed with the DNA sample and incubated
729 for 20 min at room temperature while rotating. Beads were separated on a magnet, twice
730 washed with 1x tween-washing-buffer at 55°C and 700 rpm shaking for 2 min. Reclaimed
731 beads were resuspended in 50 μ l water.

732 Sequencing library preparation: To repair DNA ends, DNA-bound beads were incubated in 100
733 μ l end-repair mix containing 1x T4 Ligase Buffer (NEB), 0.5 mM dNTP mix, 0.5 U/ μ l T4
734 Polynucleotide Kinase (NEB, M0201), 0.12 U/ μ l T4 DNA Polymerase (NEB, M0203) and 0.05
735 U/ μ l Klenow (NEB, M0210). Samples were incubated for 30 min at 20°C. Beads were
736 separated on a magnet, twice washed with 1x tween-washing-buffer at 55°C and 700 rpm
737 shaking for 2 min. Reclaimed beads were resuspended in 50 μ l water. Next, dA-tail was added
738 by incubating DNA-bound beads in 100 μ l A-tailing mix, containing 1x NEB buffer, 0.5 μ M
739 dATP, and 0.25 U/ μ l Klenow, exo- (NEB, M0212). Samples were incubated for 30 min at 37°C.
740 Beads were separated on a magnet, twice washed with 1x tween-washing-buffer at 55°C and
741 700 rpm shaking for 2 min. Reclaimed beads were resuspended in 20 μ l water. Subsequently,
742 samples were indexed by ligating TruSeq Illumina adaptors by incubating DNA-bound beads
743 in 50 μ l adapter ligation mix, containing 1x T4 Ligation buffer, 5% PEG-4000, 0.3 U/ μ l T4 DNA
744 Ligase (ThermoFisher, EL0011), 1.5 μ l TruSeq index adapter. The reaction was incubated at
745 22°C for 2 hours with occasionally mixing. Beads were separated on a magnet, twice washed
746 with 1x tween-washing-buffer at 55°C and 700 rpm shaking for 2 min. Reclaimed beads were
747 resuspended in 50 μ l water. Final library for paired-end sequencing was prepared using
748 NEBNext High-Fidelity 2X PCR Master Mix (NEB). PCR reaction: 50 μ l reaction, containing 1x
749 NEBNext High-Fidelity PCR Master Mix, 0.3 μ M TruSeq Primer 1.0 (P5) and TruSeq Primer
750 2.0 (P7), 3 μ l DNA-bound beads. PCR cycler setup: 1. 98°C for 60 seconds, 2. 98°C for 10
751 seconds, 3. 65°C for 30 seconds, 4. 72°C for 30 seconds, 5. Go to step 2 for up to 10 cycles,
752 6. 72°C for 5 min. Optimal cycle number was determined for each sample by analysing a 5 μ l
753 aliquot on an agarose gel after 4, 6, 8, 10 and 12 cycles. For each sample, at least 8
754 independent PCR reactions were performed to maintain initial library complexity and then
755 pooled for AMPure beads purification. 1.2x volume of AMPure beads were added to the

756 sample, mixed by pipetting, and incubated for 10 min at room temperature. Beads were
757 separated on a magnet, and clear supernatant was discarded. Beads were washed twice with
758 70% EtOH, and air dried for 5 min. DNA was eluted in 50 μ l water. Libraries were multiplexed
759 and sequenced using DNBseq technology to produce 50 bp paired-end reads and
760 approximately 400 million raw sequencing read pairs for each genotype.

761

762 **HiC data analyses**

763 Mapping, filtering, normalization and visualization: HiC paired-end reads were mapped to the
764 zebrafish genome assembly GRCz10 (danRer10) using BWA⁷¹. Reads from biological
765 replicates were pooled before mapping. Then, ligation events (HiC pairs) were detected and
766 sorted, and PCR duplicates were removed, using the pairtools package
767 (<https://github.com/mirnylab/pairtools>). Unligated and self-ligated events (dangling and extra-
768 dangling ends, respectively) were filtered out by removing contacts mapping to the same or
769 adjacent restriction fragments. The resulting filtered pairs file was converted to a tsv file that
770 was used as input for Juicer Tools Pre⁷², which generated multiresolution hic files. HiC matrices
771 at 10 and 500 Kb resolution, normalized with the Knight-Ruiz (KR) method⁷³, were extracted
772 for downstream analysis using the FAN-C toolkit⁷⁴. Visualization of normalized HiC matrices
773 and other values described below, such as insulation scores, TAD boundaries, aggregate TAD
774 and loop analysis, Pearson's correlation matrices and eigenvectors, were calculated and
775 visualized using FAN-C.

776 TADs, chromatin loops and compartmentalization: TAD boundaries were called using the
777 insulation score method, as previously described⁴². Insulation scores were calculated for 10-
778 Kb binned HiC matrices using FAN-C⁷⁴. Briefly, the average number of interactions of each bin
779 were calculated in 500-Kb square sliding windows (50 x 50 bins); then, these values were
780 normalized as the \log_2 ratio of each bin's value and the mean of all bins to obtain the insulation
781 score for each bin; next, minima along the insulation score vector were calculated using a delta
782 vector of +/-100 Kb (+/-10 bins) around the central bin; finally, boundaries with scores lower
783 than 0.5 were filtered out. The genomic regions located between adjacent boundaries were
784 considered as TADs.

785 For determination of A and B compartments, 500-Kb binned HiC matrices were used.
786 Pearson's correlation matrices were calculated as previously described⁷⁵, using FAN-C⁷⁴. A/B
787 compartments and their strength were determined using the 2nd eigenvector, since the 1st
788 eigenvector corresponded with chromosome arms in our system, and the genome GC content.
789 A/B domains were defined as consecutive regions with the same eigenvector sign. A/B

790 enrichment profiles were calculated by dividing bins in fifty percentiles according to their 2nd
791 eigenvector values and plotting their average observed/expected contact values.

792 Chromatin loops were called using HICCUPS¹⁰, with standard parameters. Briefly, the
793 multiresolution hic file was used as input for the CPU version of HICCUPS, which run using 5,
794 10 and 25-Kb resolution KR-normalized matrices. The maximum permitted FDR value was 0.1
795 for the three resolutions; the peak widths were 4, 2 and 1 bin for 5, 10 and 25-Kb resolutions,
796 respectively; and the window widths to define the local neighborhoods used as background
797 were 7, 5 and 3 bins, respectively. The thresholds for merging loop lists from different
798 resolutions were the following: maximum sum of FDR values of 0.02 for the horizontal, vertical,
799 donut and lower-left neighborhoods; minimum enrichment of 1.5 for the horizontal and vertical
800 neighborhoods; minimum enrichment of 1.75 for the donut and bottom-left neighborhoods;
801 minimum enrichment of 2 for either the donut or the bottom-left neighborhoods. The distances
802 used to merge the nearby pixels to a centroid were 20, 20 and 50-Kb for 5, 10 and 25-Kb
803 resolutions, respectively. CTCF-bound and chromatin loops were considered when at least
804 one of the loop anchors overlapped with a CTCF ChIP-seq peak.

805

806 **UMI-4C**

807 UMI-4C library preparation was performed as previously described⁷⁶ with modifications in 3C
808 library preparation and minor modification in sequencing library preparation. Experiments were
809 performed in singletons in wild-type and *ctcf*^{-/-} mutant embryos at 48 hpf, using one to three
810 million cells as input material. Embryo fixation, nuclei extraction, chromatin digestion, biotin fill-
811 in, proximity ligation, cross-link reversal, and DNA purification were performed following above
812 experimental procedure for HiC. The following procedure were specific for UMI-4C.

813 DNA shearing: 5-7 μ g of purified DNA was sheared with Covaris M220 sonicator with the
814 following setup: 130 μ l sample volume, Peak Incident Power (W): 50, Duty Factor: 10%, Cycles
815 per Burst: 200, Treatment Time (s): 70, cooling at 7°C. Samples were then purified using
816 AMPure XP beads (Agencourt, A63881) as follows: 2.0x volume of AMPure beads were added
817 to the sample, mixed by pipetting, and incubated for 10 min at room temperature. Beads were
818 separated on a magnet, and clear supernatant was discarded. Beads were washed twice with
819 70% EtOH, and air dried for 5 min. DNA was eluted in 300 μ l water.

820 Biotin pull down: Biotin-labelled DNA was bound to Dynabeads My One C1 Streptavidin beads,
821 using 5 μ l of beads per 1 μ g DNA and following manufacturer's instructions. Beads were
822 washed twice with 1x tween-washing-buffer (5 mM Tris HCl pH 7.5, 0.5 mM EDTA, 1 M NaCl,
823 0.05% Tween 20) and finally resuspended in 1x sample volume 2x binding buffer (10 mM Tris
824 HCl pH 7.5, 1 mM EDTA, 2 M NaCl). Beads were mixed with the DNA sample and incubated

825 for 20 min at room temperature while rotating. Beads were separated on a magnet, twice
826 washed with 1x tween-washing-buffer at 55°C and 700 rpm shaking for 2 min. Reclaimed
827 beads were resuspended in 50 μ l water.

828 Sequencing library preparation: 500 ng of DNA attached to beads were end-repaired by
829 incubating in 100 μ l end-repair mix (1x T4 Ligase Buffer (NEB), 0.5 mM dNTP mix, 0.12 U/ μ l
830 T4 DNA Polymerase (NEB, M0203) and 0.05 U/ μ l Klenow (NEB, M0210)) for 30 min at 20°C.
831 Beads were separated on a magnet, twice washed with 1x tween-washing-buffer at 55°C and
832 700 rpm shaking for 2 min. Reclaimed beads were resuspended in 50 μ l water. Next, DNA-
833 bound beads were incubated for 30 min at 37°C in 100 μ l A-tailing mix (1x NEB buffer, 0.5 μ M
834 dATP, and 0.25 U/ μ l Klenow, exo- (NEB, M0212)). The enzyme was heat inactivated at 75°C
835 for 20 min. For 5' dephosphorylation of DNA ends, 2 μ l of Alkaline Phosphatase, Calf Intestinal
836 (NEB, M0290) was added and samples were incubated at 37°C for 1 hour and with
837 occasionally mixing. Beads were separated on a magnet, twice washed with 1x tween-
838 washing-buffer at 55°C and 700 rpm shaking for 2 min. Reclaimed beads were resuspended
839 in 20 μ l water. Next, samples were indexed by ligating TruSeq Illumina adaptors by incubating
840 DNA-bound beads in 50 μ l adapter ligation mix (1x T4 Ligation buffer, 5% PEG-4000, 0.3 U/
841 μ l T4 DNA Ligase (ThermoFisher, EL0011), 1.5 μ l TruSeq index adapter). The reaction was
842 incubated at 22°C for 2 hours with occasionally mixing. Sample volume was increased with
843 water to a total 100 μ l and incubated at 96°C for 5 min to denature DNA and remove non-
844 ligated strand from adapter. Sample were placed on ice and beads were separated on a
845 magnet, twice washed with 1x tween-washing-buffer at 55°C and 700 rpm shaking for 2 min.
846 Reclaimed beads were resuspended in 20 μ l water. Final library for paired-end sequencing
847 was prepared using NEBNext High-Fidelity 2X PCR Master Mix (NEB) and a nested PCR
848 approach as described in Schwartzman et al. 2016. Individual viewpoints are defined by US
849 (upstream) and DS (downstream) primers within the DpnII fragment of interest ([Supplementary](#)
850 [Table 1](#)). US and DS primers were designed with melting temperature of 58°C. DS primers
851 were designed between 5-15 bp from the interrogated DpnII restriction site and containing P5
852 sequence at their 5' end. US primers were designed within a region of up to 100 bp of
853 interrogated DpnII restriction site and with only minimal overlap with DS primers. Up to 14 US
854 and DS primers were pooled for multiplex PCR reaction, respectively. First PCR reaction: 50
855 μ l reaction, containing 1x NEBNext High-Fidelity 2X PCR Master Mix, 0.3 μ M US primer mix
856 (each) and 0.3 μ M TruSeq Primer 2.0 (P7), 200 ng DNA-bound on beads. PCR cycler setup:
857 1. 98°C for 30 seconds, 2. 98°C for 10 seconds, 3. 58°C for 30 seconds, 4. 72°C for 60
858 seconds, 5. Go to step 2 for 18 cycles in total, 6. 72°C for 5 min. For each sample two PCR
859 reactions were performed and then pooled for AMPure beads purification. 1.2x volume of

860 AMPure beads were added to the sample, mixed by pipetting, and incubated for 10 min at
861 room temperature. Beads were separated on a magnet, and clear supernatant was discarded.
862 Beads were washed twice with 70% EtOH, air dried, and DNA was eluted in 30 μ l water.
863 Second PCR reaction: 50 μ l reaction, containing 1x NEBNext High-Fidelity 2X PCR Master
864 Mix, 0.3 μ M DS primer mix (each) and 0.3 μ M TruSeq Primer 2.0 (P7), 100 ng DNA from first
865 PCR. PCR cycler setup: Corresponded to setup of first PCR but with 15 cycles. For each
866 sample 3-5 PCR reactions were performed and then pooled for size selection for fragments
867 between 200 and 700 bp, using AMPure beads. 0.575x volume of AMPure beads were added
868 to the sample, mixed by pipetting, and incubated for 10 min at room temperature. Beads were
869 separated on a magnet, and clear supernatant was transferred to a fresh tube. 0.3x volume of
870 fresh AMPure beads were added to the supernatant, mixed, and incubated for 10 min at room
871 temperature. Beads were separated on a magnet, and clear supernatant was discarded.
872 Beads were washed twice with 70% EtOH, and air dried for 5 min. DNA was eluted in 300 μ l
873 water. Libraries were multiplexed and sequenced using DNBseq technology to produce 50 bp
874 paired-end reads and approximately 1-5 million raw sequencing read pairs for each viewpoint
875 and genotype.

876 For the UMI-4C data analysis, raw fastq files were processed using the R package
877 umi4cpackage (<https://bitbucket.org/tanaylab/umi4cpackage>). Contact profiles and
878 domainograms were generated using the default parameters and a minimum win_cov of 10.

879

880 **Statistical analyses**

881 For comparison of insulation scores, TAD sizes, loop ranges and expression fold-changes
882 among datasets, two-tailed Wilcoxon's rank sum tests were used. In [Fig. 3f](#) and [Supplementary](#)
883 [Fig. 7](#), box plots represent: center line, median; box limits, upper and lower quartiles; whiskers,
884 1.5x interquartile range; notches, 95% confidence interval of the median. Other boxplots
885 represent the same parameters but do not include notches. Statistical significance of
886 contingency tables was assessed using the Fisher's exact test.

887

888 **Data availability**

889 HiC, ChIPmentation, RNA-seq, ATAC-seq and UMI-4C data generated in this study are
890 available through the Gene Expression Omnibus (GEO) accession number GSE156099
891 [<https://www.ncbi.nlm.nih.gov/geo/query/acc.cgi?acc=GSE156099>].

892

893 **Code availability**

894 Custom code used in this study is available at the Gitlab repository:
895 https://gitlab.com/rdacemel/hic_ctcf-null.

896

897 **Methods' References**

- 898 51 Moreno-Mateos, M. A. *et al.* CRISPRscan: designing highly efficient sgRNAs for
899 CRISPR-Cas9 targeting in vivo. *Nat Methods* **12**, 982-988, doi:10.1038/nmeth.3543
900 (2015).
- 901 52 Carmona-Aldana, F. *et al.* CTCF knockout reveals an essential role for this protein
902 during the zebrafish development. *Mech Dev* **154**, 51-59,
903 doi:10.1016/j.mod.2018.04.006 (2018).
- 904 53 Freitas, R., Gomez-Marin, C., Wilson, J. M., Casares, F. & Gomez-Skarmeta, J. L.
905 Hoxd13 contribution to the evolution of vertebrate appendages. *Dev Cell* **23**, 1219-
906 1229, doi:10.1016/j.devcel.2012.10.015 (2012).
- 907 54 Tena, J. J. *et al.* Odd-skipped genes encode repressors that control kidney
908 development. *Dev Biol* **301**, 518-531, doi:10.1016/j.ydbio.2006.08.063 (2007).
- 909 55 Dobin, A. *et al.* STAR: ultrafast universal RNA-seq aligner. *Bioinformatics* **29**, 15-21,
910 doi:10.1093/bioinformatics/bts635 (2013).
- 911 56 Anders, S., Pyl, P. T. & Huber, W. HTSeq--a Python framework to work with high-
912 throughput sequencing data. *Bioinformatics* **31**, 166-169,
913 doi:10.1093/bioinformatics/btu638 (2015).
- 914 57 Love, M. I., Huber, W. & Anders, S. Moderated estimation of fold change and
915 dispersion for RNA-seq data with DESeq2. *Genome Biol* **15**, 550,
916 doi:10.1186/s13059-014-0550-8 (2014).
- 917 58 Huang da, W., Sherman, B. T. & Lempicki, R. A. Systematic and integrative analysis
918 of large gene lists using DAVID bioinformatics resources. *Nat Protoc* **4**, 44-57,
919 doi:10.1038/nprot.2008.211 (2009).
- 920 59 Buenrostro, J. D., Giresi, P. G., Zaba, L. C., Chang, H. Y. & Greenleaf, W. J.
921 Transposition of native chromatin for fast and sensitive epigenomic profiling of open
922 chromatin, DNA-binding proteins and nucleosome position. *Nat Methods* **10**, 1213-
923 1218, doi:10.1038/nmeth.2688 (2013).
- 924 60 Fernandez-Minan, A., Bessa, J., Tena, J. J. & Gomez-Skarmeta, J. L. Assay for
925 transposase-accessible chromatin and circularized chromosome conformation
926 capture, two methods to explore the regulatory landscapes of genes in zebrafish.
927 *Methods Cell Biol* **135**, 413-430, doi:10.1016/bs.mcb.2016.02.008 (2016).
- 928 61 Santos-Pereira, J. M., Gallardo-Fuentes, L., Neto, A., Acemel, R. D. & Tena, J. J.
929 Pioneer and repressive functions of p63 during zebrafish embryonic ectoderm
930 specification. *Nat Commun* **10**, 3049, doi:10.1038/s41467-019-11121-z (2019).
- 931 62 Schmidl, C., Rendeiro, A. F., Sheffield, N. C. & Bock, C. ChIPmentation: fast, robust,
932 low-input ChIP-seq for histones and transcription factors. *Nat Methods* **12**, 963-965,
933 doi:10.1038/nmeth.3542 (2015).
- 934 63 Langmead, B. & Salzberg, S. L. Fast gapped-read alignment with Bowtie 2. *Nat*
935 *Methods* **9**, 357-359, doi:10.1038/nmeth.1923 (2012).
- 936 64 Li, H. *et al.* The Sequence Alignment/Map format and SAMtools. *Bioinformatics* **25**,
937 2078-2079, doi:10.1093/bioinformatics/btp352 (2009).
- 938 65 Quinlan, A. R. & Hall, I. M. BEDTools: a flexible suite of utilities for comparing
939 genomic features. *Bioinformatics* **26**, 841-842, doi:10.1093/bioinformatics/btq033
940 (2010).
- 941 66 Haeussler, M. *et al.* The UCSC Genome Browser database: 2019 update. *Nucleic*
942 *Acids Res* **47**, D853-D858, doi:10.1093/nar/gky1095 (2019).
- 943 67 Zhang, Y. *et al.* Model-based analysis of ChIP-Seq (MACS). *Genome Biol* **9**, R137,
944 doi:10.1186/gb-2008-9-9-r137 (2008).

- 945 68 Ramirez, F. *et al.* deepTools2: a next generation web server for deep-sequencing
946 data analysis. *Nucleic Acids Res* **44**, W160-165, doi:10.1093/nar/gkw257 (2016).
947 69 Heinz, S. *et al.* Simple combinations of lineage-determining transcription factors prime
948 cis-regulatory elements required for macrophage and B cell identities. *Mol Cell* **38**,
949 576-589, doi:10.1016/j.molcel.2010.05.004 (2010).
950 70 Hiller, M. *et al.* Computational methods to detect conserved non-genic elements in
951 phylogenetically isolated genomes: application to zebrafish. *Nucleic Acids Res* **41**,
952 e151, doi:10.1093/nar/gkt557 (2013).
953 71 Li, H. & Durbin, R. Fast and accurate short read alignment with Burrows-Wheeler
954 transform. *Bioinformatics* **25**, 1754-1760, doi:10.1093/bioinformatics/btp324 (2009).
955 72 Durand, N. C. *et al.* Juicer Provides a One-Click System for Analyzing Loop-
956 Resolution Hi-C Experiments. *Cell Syst* **3**, 95-98, doi:10.1016/j.cels.2016.07.002
957 (2016).
958 73 Knight, P. A. & Ruiz, D. A fast algorithm for matrix balancing. *IMA Journal of*
959 *Numerical Analysis* **33**, 1029-1047, doi:10.1093/imanum/drs019 (2012).
960 74 Kruse, K., Hug, C. B. & Vaquerizas, J. M. FAN-C: A Feature-rich Framework for the
961 Analysis and Visualisation of C data. *bioRxiv*, 2020.2002.2003.932517,
962 doi:10.1101/2020.02.03.932517 (2020).
963 75 Lieberman-Aiden, E. *et al.* Comprehensive mapping of long-range interactions
964 reveals folding principles of the human genome. *Science* **326**, 289-293,
965 doi:10.1126/science.1181369 (2009).
966 76 Schwartzman, O. *et al.* UMI-4C for quantitative and targeted chromosomal contact
967 profiling. *Nat Methods* **13**, 685-691, doi:10.1038/nmeth.3922 (2016).
968

969

970 **Acknowledgements**

971 We thank C. Paliou and J. López-Ríos for critical reading of the manuscript; C. Bolt and L.
972 Delisle from the Duboule lab for technical advice with the UMI-4C protocol; F. Rencillas-Targa
973 for providing the zebrafish-specific CTCF antibody; the CABD Fish and Microscopy Facilities
974 for technical assistance; and C3UPO for the HPC support. JLG-S received funding from the
975 ERC (Grant Agreement No. 740041), the Spanish Ministerio de Economía y Competitividad
976 (Grant No. BFU2016-74961-P) and the institutional grant Unidad de Excelencia María de
977 Maeztu (MDM-2016-0687). JT was funded by a 2019 Leonardo Grant for Researchers and
978 Cultural Creators, BBVA Foundation. MF was funded by the European Union's Horizon 2020
979 research and innovation programme under the Marie Skłodowska-Curie grant agreement
980 [#800396] and a Juan de la Cierva-Formación fellow from the Spanish Ministry of Science and
981 Innovation (FJC2018-038233-I).

982

983 **Author contributions**

984 MF, JMS-P and JLG-S conceived and designed the project; EC-M, MF, AN and JMS-P
985 performed the experiments; JMS-P, MF, RDA and JJT analyzed the data; MF, JMS-P and
986 JLG-S wrote the manuscript.

987

988 **Competing interests**

989 The authors declare no conflict of interests.

990

991 **Correspondence and requests for materials** should be addressed to JMS-P.

992

993 **SUPPLEMENTARY MATERIAL**

994

995 **Supplementary Table 1 – List of primers used in this study**

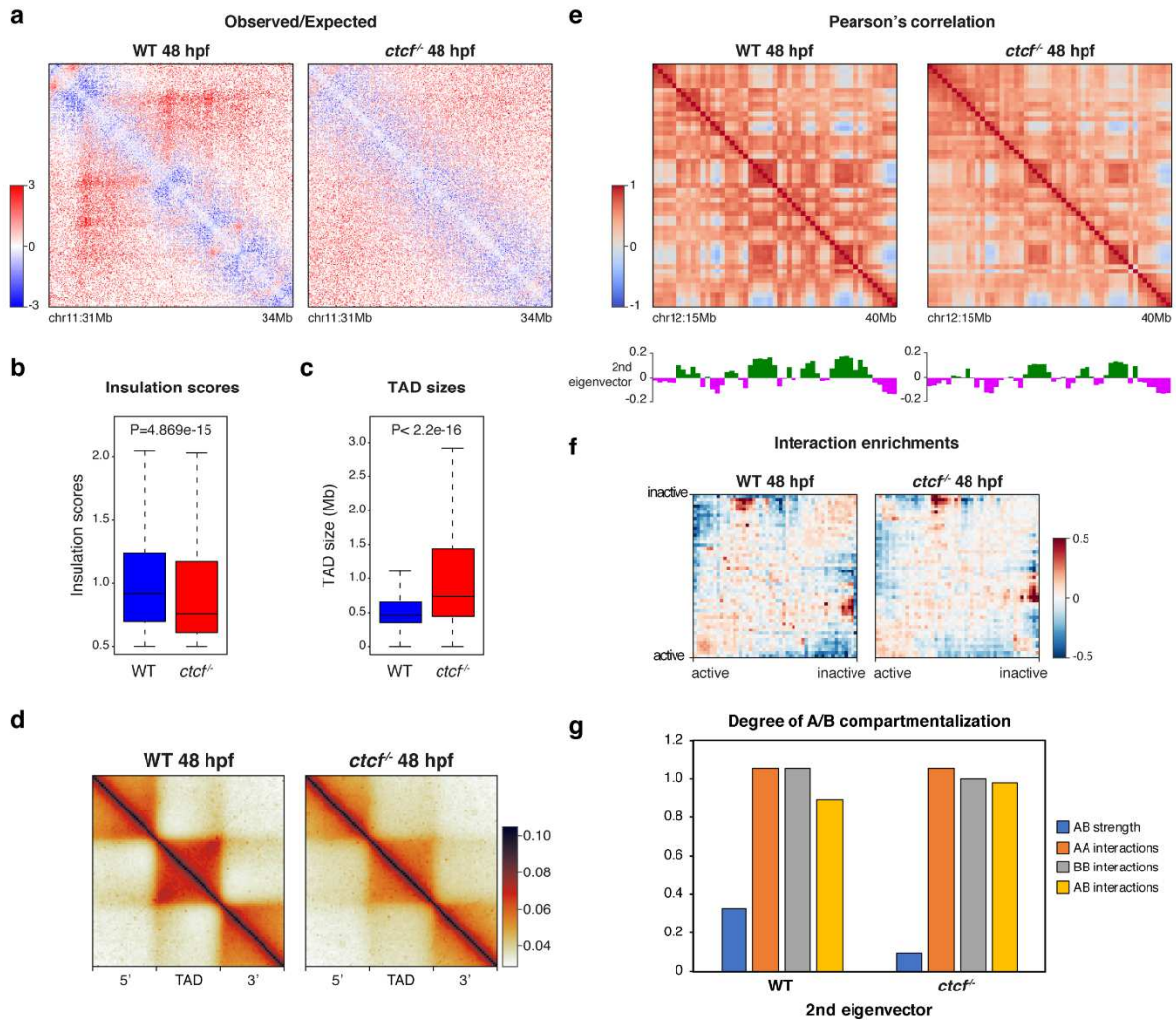
996

Primer name	Primer sequence
CTCFexon4	5'-AATACGACTCACTATAGGAGTTACTTGTCCACGCGTTTTA GAGCTAGAA_3'
CTCFexon5	5'-TAATACGACTCACTATAGGCATGGCCTTTGTCACCAGGTTTT AGAGCTAGAA-3'
sgRNA_univ	5'-AAAAGCACCGACTCGGTGCCACTTTTTCAAGTTGATAACGGA CTAGCCTTATTTTAACTTGCTATTTCTAGCTCTAAAC-3'
CTCFpF	5'-CAAGCTGCGCTACAACACAG-3'
CTCFpR	5'-CTCCTGTGTGGGAGCGAATG-3'
ptch2F	5'-TCCTGTGCTGTTTCTACAGG-3'
ptch2R	5'-GGATCCATTAACCCTCACTAAAGGGAATGCGCAGAACAAGTTATAGG-3'
hoxa5aF	5'-GGCGTGGACTATCCCTTAC-3'
hoxa5aR	5'-GGATCCATTAACCCTCACTAAAGGGAAGGAGGCCAATCACACCTTAC-3'
hoxa9aF	5'-CCCTTCCCTCTACCTTTTCC-3'
hoxa9aR	5'-GGATCCATTAACCCTCACTAAAGGGAAGAAGGTCAACAGACCATGAGG-3'
hoxc1aF	5'-GTCTGTGGATGGAGTTTCG-3'
hoxc1aR	5'-GGATCCATTAACCCTCACTAAAGGGAAGGTGCTTTAACGGTACGTG-3'
umi4C-ptch2- US	5'-CATCAAACCACCCTTTTCAG-3'
umi4C-ptch2- DS	5'-AATGATACGGCGACCACCGAGATCTACACTCTTTCCCTACACGACGCTCTTCC GATCTGGGCTACCTCTCCAAATGTT-3'
umi4C- hoxd4a-US	5'-TTTCCTACCTTCAGAAATTAATGG-3'
umi4C- hoxd4a-DS	5'-AATGATACGGCGACCACCGAGATCTACACTCTTTCCCTACACGACGCTCTTCC GATCTTCGTACATGGTGAATCCAA-3'
umi4C- hoxd13a-US	5'-GAGCGTGAATACAACACCACTA-3'
umi4C- hoxd13a-DS	5'-AATGATACGGCGACCACCGAGATCTACACTCTTTCCCTACACGACGCTCTTCC GATCTCCACTAAGTTCATTACAAAGGAGA-3'

997

998

999



1000

1001

1002

1003

1004

1005

1006

1007

1008

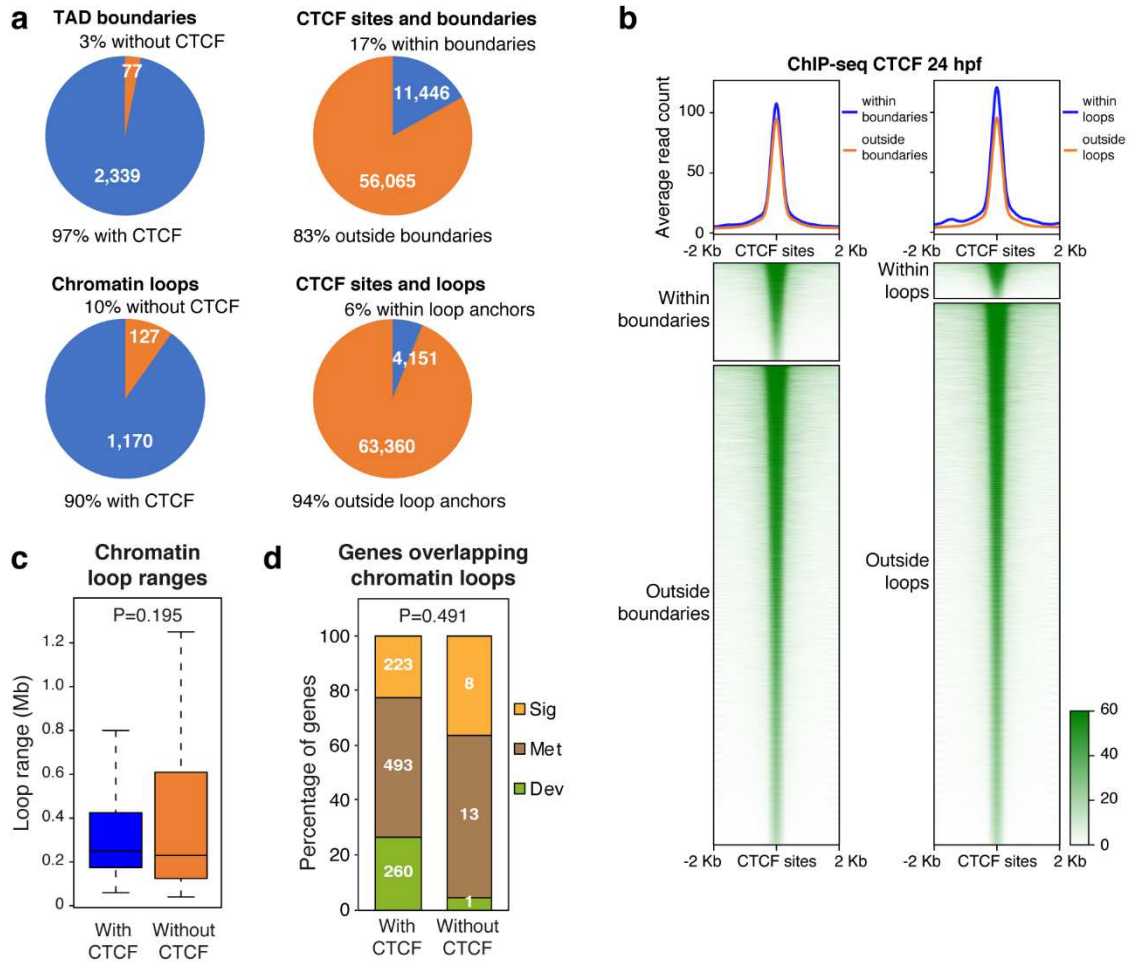
1009

1010

1011

1012

Supplementary Figure 1. Chromatin structure in zebrafish embryos requires CTCF. **a**, HiC observed/expected contact maps at 10 Kb resolution in WT and *ctcf*^{-/-} zebrafish embryos at 48 hpf. The 3-Mb genomic region shown in Figure 1c is plotted. **b-c**, Box plots showing the insulation scores of the TAD boundaries (**b**) and the TAD sizes (**c**) in WT and *ctcf*^{-/-} embryos at 48 hpf. Statistical significance was assessed using the Wilcoxon's rank sum test. **d**, Aggregate analysis of normalized HiC signal in WT and *ctcf*^{-/-} embryos at 48 hpf for the 2,438 TADs called in WT embryos, rescaled and surrounded by windows of the same size. **e**, Pearson's correlation matrices from HiC data at 500 Kb resolution in WT and *ctcf*^{-/-} embryos at 48 hpf. A 25-Mb genomic region is plotted, aligned with the 2nd eigenvector demarcating A and B compartments. **f**, Saddle plots showing the genome-wide interaction enrichments between active and inactive genomic regions from HiC data in WT and *ctcf*^{-/-} embryos at 48 hpf. **g**, Bar plots showing the degree of compartmentalization in WT and *ctcf*^{-/-} embryos at 48 hpf. AB strength and quantification of AA, BB and AB interactions based in the 2nd eigenvector, are plotted.



1013

1014

1015

1016

1017

1018

1019

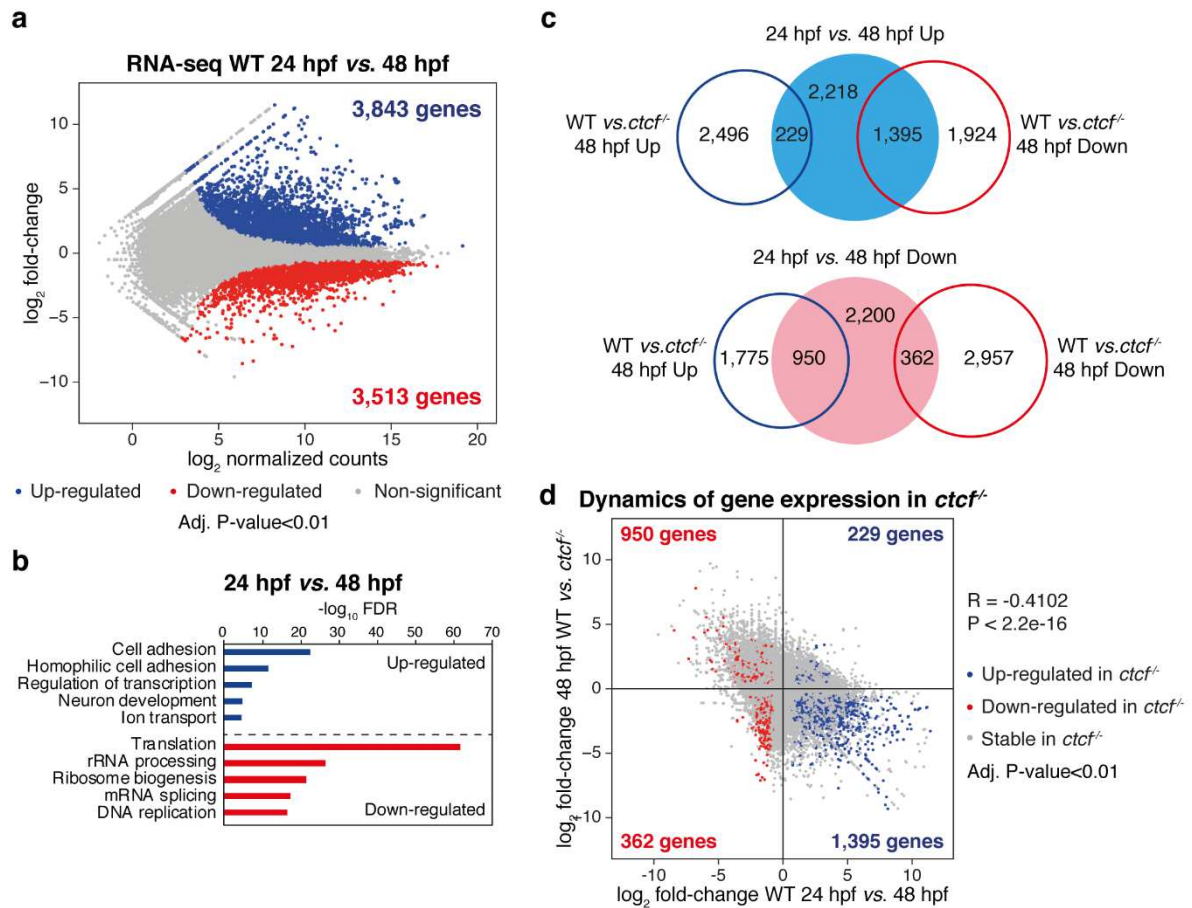
1020

1021

1022

1023

Supplementary Figure 2. CTCF is bound to TAD boundaries and chromatin loops in zebrafish embryos. a, Pie charts showing the percentage of TADs or chromatin loops overlapping with CTCF sites (left) and the percentage of CTCF sites overlapping with TADs or chromatin loops (right). **b,** Heatmaps and average profiles of CTCF ChIP-seq signal at CTCF sites overlapping or not with TADs or chromatin loops. **c,** Box plots showing the distance between loop anchors (loop ranges) for the chromatin loops overlapping or not with CTCF sites at least in one of their anchors. Statistical significance was assessed using the Wilcoxon's rank sum test. **d,** Proportion of genes annotated to the GO terms "Signaling", "Metabolic process" and "Developmental process" for genes overlapping with chromatin loop anchors, with or without CTCF binding. Statistical significance was assessed using the Fisher's exact test.



1024

1025

1026

1027

1028

1029

1030

1031

1032

1033

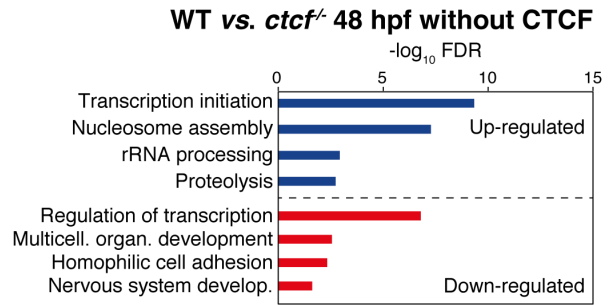
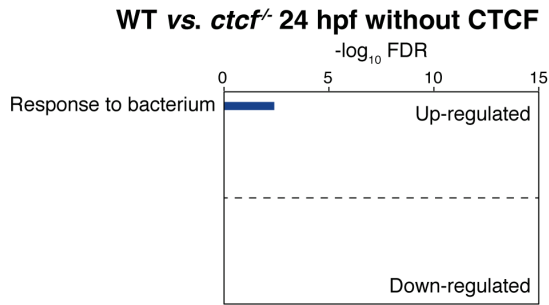
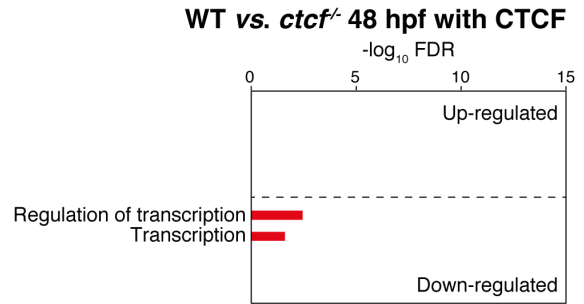
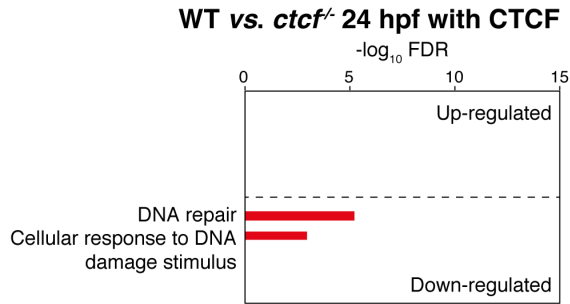
1034

1035

1036

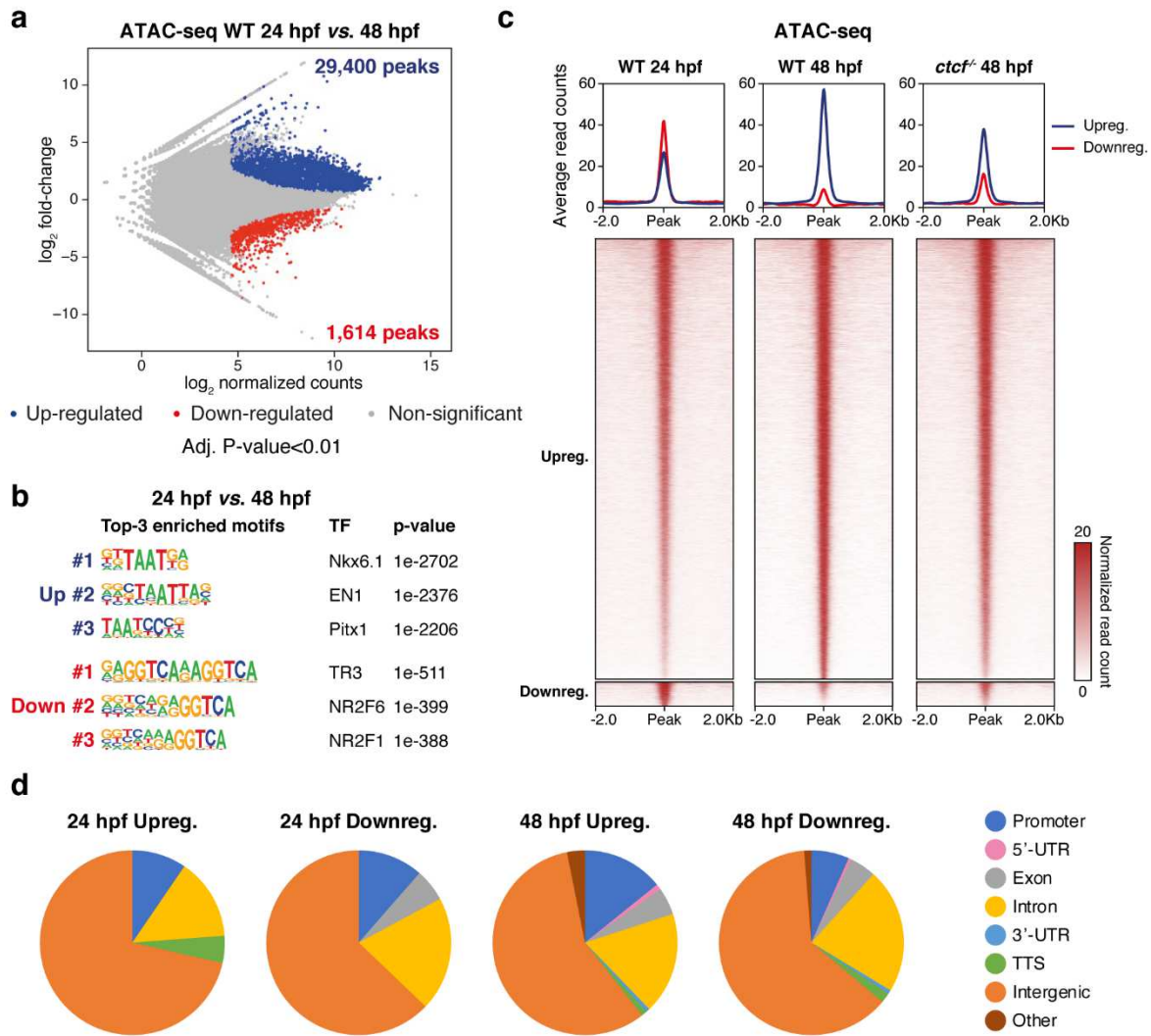
1037

Supplementary Figure 3. CTCF is required for dynamic expression changes during development. **a**, Differential analysis of gene expression in WT embryos between 24 and 48 hpf from RNA-seq data (n = 2 biological replicates per condition). The log₂ normalized read counts of 24-hpf transcripts versus the log₂ fold-change of expression are plotted. Transcripts showing a statistically significant differential expression (adjusted P-value < 0.01) are highlighted in blue (up-regulated) or red (down-regulated). The number of genes that correspond to the up- and down-regulated transcripts are shown inside the boxes. **b**, GO enrichment analyses of biological processes for the up- and down-regulated genes in WT embryos from 24 to 48 hpf. Terms showing an FDR < 0.05 are considered as enriched. **c**, Venn diagrams showing the overlap between the genes up- and down-regulated in WT embryos from 24 to 48 hpf and the genes up- and down-regulated in *ctcf*^{-/-} embryos at 48 hpf (see Fig. 2b). **d**, Scatter plots showing the correlation between the expression fold change of all transcripts in WT embryos from 24 to 48 hpf, and their expression fold change in *ctcf*^{-/-} embryos at 48 hpf. Up- and down-regulated transcripts in *ctcf*^{-/-} embryos are highlighted in blue or red, respectively.



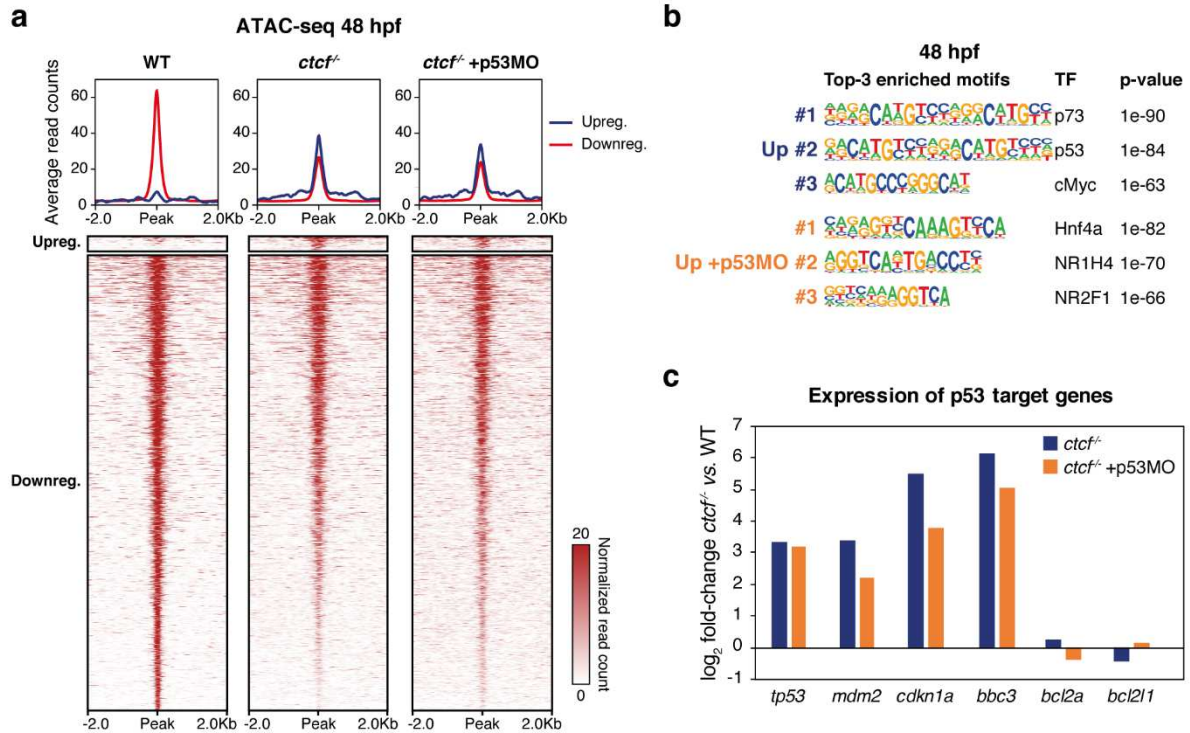
1038
1039
1040
1041
1042
1043

Supplementary Figure 4. CTCF absence leads to down-regulation of developmental genes. GO enrichment analyses of biological processes for the up- and down-regulated genes in *ctcf*^{-/-} embryos at 24 (left) and 48 hpf (right), distinguishing between those genes with (top) or without (bottom) CTCF binding at their TSS. Terms showing a false discovery rate (FDR) < 0.05 are considered as enriched.



1044

1045 **Supplementary Figure 5. The dynamics of the chromatin accessibility landscape requires CTCF.** **a**,
 1046 Differential analysis of chromatin accessibility in WT embryos between 24 and 48 hpf from ATAC-seq data (n = 2
 1047 biological replicates per condition). The log₂ normalized read counts of 24-hpf ATAC peaks versus the log₂ fold-
 1048 change of accessibility are plotted. Regions showing a statistically significant differential accessibility (adjusted P-
 1049 value < 0.01) are highlighted in blue (up-regulated) or red (down-regulated). The number of peaks that correspond
 1050 to the up- and down-regulated sites are shown inside the boxes. **b**, Motif enrichment analyses for the up- and down-
 1051 regulated ATAC peaks in WT embryos from 24 to 48 hpf. The 3 motifs with the lowest p-values are shown for each
 1052 case. **c**, Heatmaps and average profiles plotting normalized ATAC-seq signal in WT embryos at 24 and 48 hpf and
 1053 in *ctcf*^{-/-} embryos at 48 hpf for the up- and down-regulated peaks from (a). **d**, Pie charts showing the annotation to
 1054 different genomic features of ATAC-peaks up- or down-regulated in *ctcf*^{-/-} embryos at 24 or 48 hpf (see Fig. 3a-b).
 1055



1056

1057

1058

1059

1060

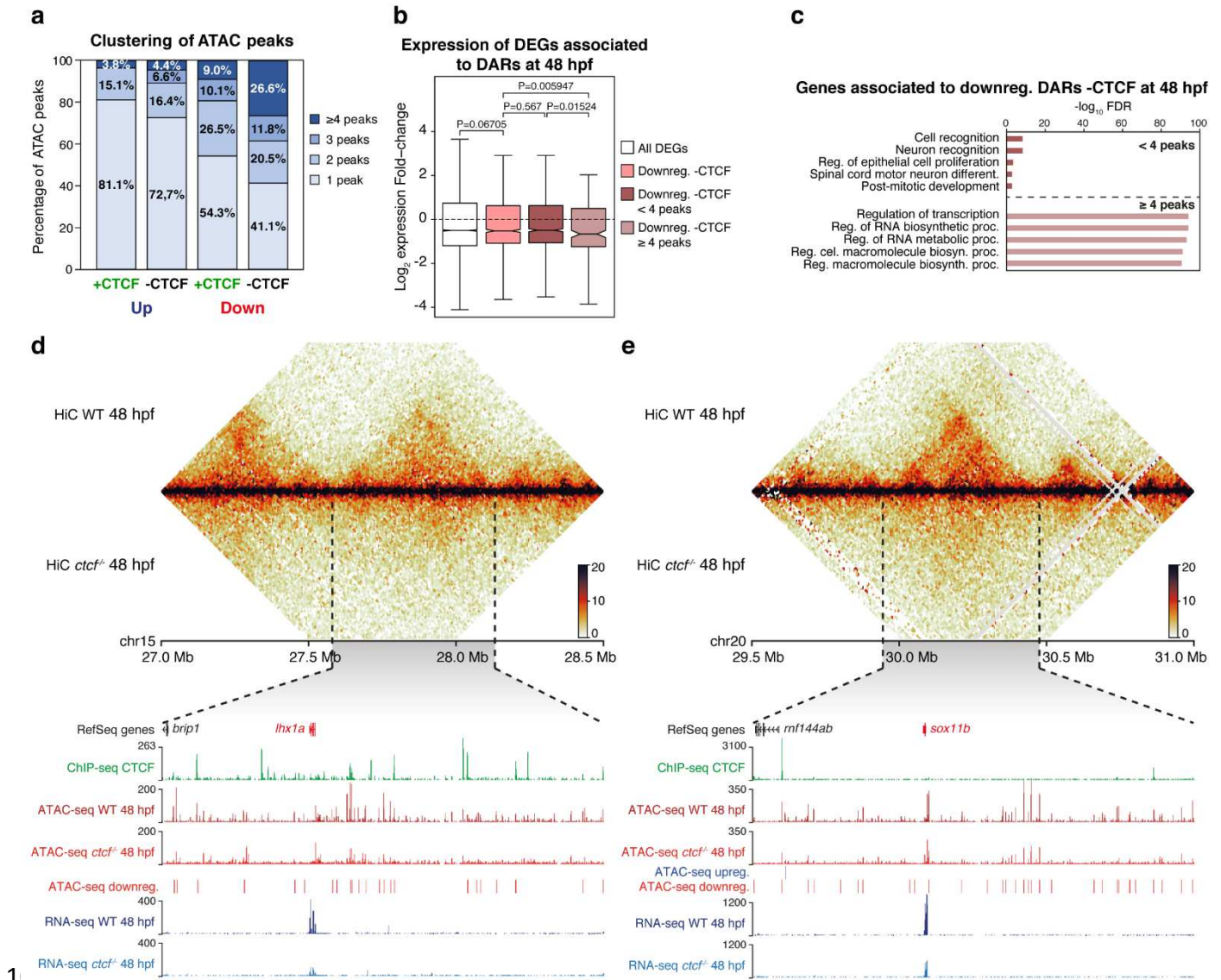
1061

1062

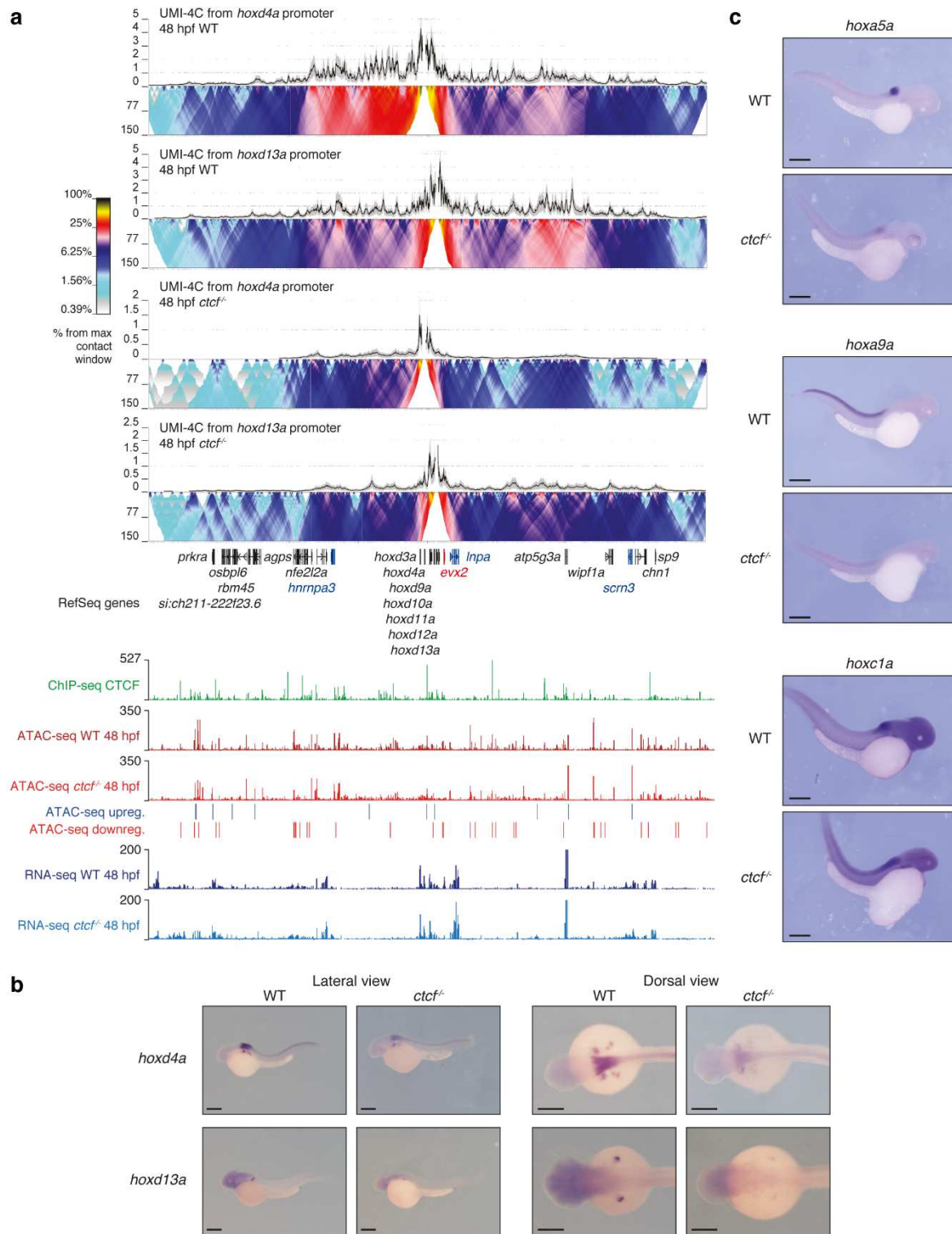
1063

1064

Supplementary Figure 6. The p53 pro-apoptotic response in the absence of CTCF does not suppress defects in chromatin accessibility. **a**, Heatmaps and average profiles plotting normalized ATAC-seq signal in WT, control *ctcf*^{-/-} and p53 morpholino (p53MO)-injected *ctcf*^{-/-} embryos at 48 hpf for the up- and down-regulated peaks in control *ctcf*^{-/-} embryos (see Fig. 3b). **b**, Motif enrichment analyses for the up-regulated ATAC peaks in control *ctcf*^{-/-} and p53MO-injected *ctcf*^{-/-} embryos at 48 hpf. The 3 motifs with the lowest p-values are shown for each case. **c**, Gene expression fold change from RNA-seq data of the *tp53* gene and the p53 target genes *mdm2*, *cdkn1a*, *bbc3*, *bcl2a* and *bcl2l1*, in control *ctcf*^{-/-} and p53MO-injected *ctcf*^{-/-} embryos at 48 hpf.



1066 **Supplementary Figure 7. CTCF loss reduces accessibility at clustered *cis*-regulatory elements around**
 1067 **developmental genes.** **a**, Bar plots showing the level of clustering of the up- and down-regulated ATAC-seq peaks
 1068 in *ctcf*^{-/-} embryos at 48 hpf, with or without CTCF binding. Peaks were considered to be clustered when located less
 1069 than 30 Kb from each other. **b**, Box plots showing the expression fold-change in *ctcf*^{-/-} embryos at 48 hpf of all DEGs
 1070 or only those associated with down-regulated DARs not overlapping with CTCF sites, grouped in less or more than
 1071 4 peaks per cluster. Center line, median; box limits, upper and lower quartiles; whiskers, 1.5x interquartile range;
 1072 notches, 95% confidence interval of the median Statistical significance was assessed using the Wilcoxon's rank
 1073 sum test. **c**, GO enrichment analyses of biological processes for the genes associated with the down-regulated
 1074 DARs in *ctcf*^{-/-} embryos at 48 hpf not overlapping with CTCF sites, grouped in less or more than 4 peaks per cluster.
 1075 Top-5 terms showing an FDR < 0.05 are considered as enriched. **d**, Top, heatmaps showing HiC signal in WT and
 1076 *ctcf*^{-/-} embryos at 48 hpf in a 1.5-Mb region of chromosomes 15 (left) or 20 (right). Bottom, zoom within the *lhx1a*
 1077 TAD (left) or the *sox11b* TAD (right) showing UCSC Genome Browser tracks with CTCF ChIP-seq, ATAC-seq at
 1078 48 hpf in WT and *ctcf*^{-/-} embryos, ATAC-seq up- or down-regulated peaks and RNA-seq at 48 hpf in WT and
 1079 *ctcf*^{-/-} embryos. The down-regulated genes are shown in red.
 1080



1081

1082

1083

1084

1085

1086

1087

1088

1089

1090

1091

1092

Supplementary Figure 8. CTCF is required for the establishment of regulatory landscapes at the HoxD locus and *hox* gene expression. **a**, Top, UMI-4C assays in WT and *ctcf*^{-/-} embryos at 48 hpf using the *hoxd4a* and *hoxd13a* gene promoters as viewpoints. Black lines and grey shadows represent the average normalized UMI counts and their standard deviation, respectively. Domainograms below UMI counts represent contact frequency between pairs of genomic regions. Bottom, UCSC Genome Browser tracks with CTCF ChIP-seq, ATAC-seq at 48 hpf in WT and *ctcf*^{-/-} embryos, ATAC-seq up- and down-regulated peaks and RNA-seq at 48 hpf in WT and *ctcf*^{-/-} embryos. Up- and down-regulated genes are shown in blue and red, respectively. **b**, Whole-mount *in situ* hybridization of the *hoxd4a* and *hoxd13a* genes in WT and *ctcf*^{-/-} embryos at 48 hpf. Left, lateral view; right, dorsal view. Anterior is to the left and scale bars represent 500 μ m. **c**, Whole-mount *in situ* hybridization of the *hoxa5a*, *hoxa9a* and *hoxc1a* genes in WT and *ctcf*^{-/-} embryos at 48 hpf. Left, Anterior is to the right and scale bars represent 500 μ m.

Figures

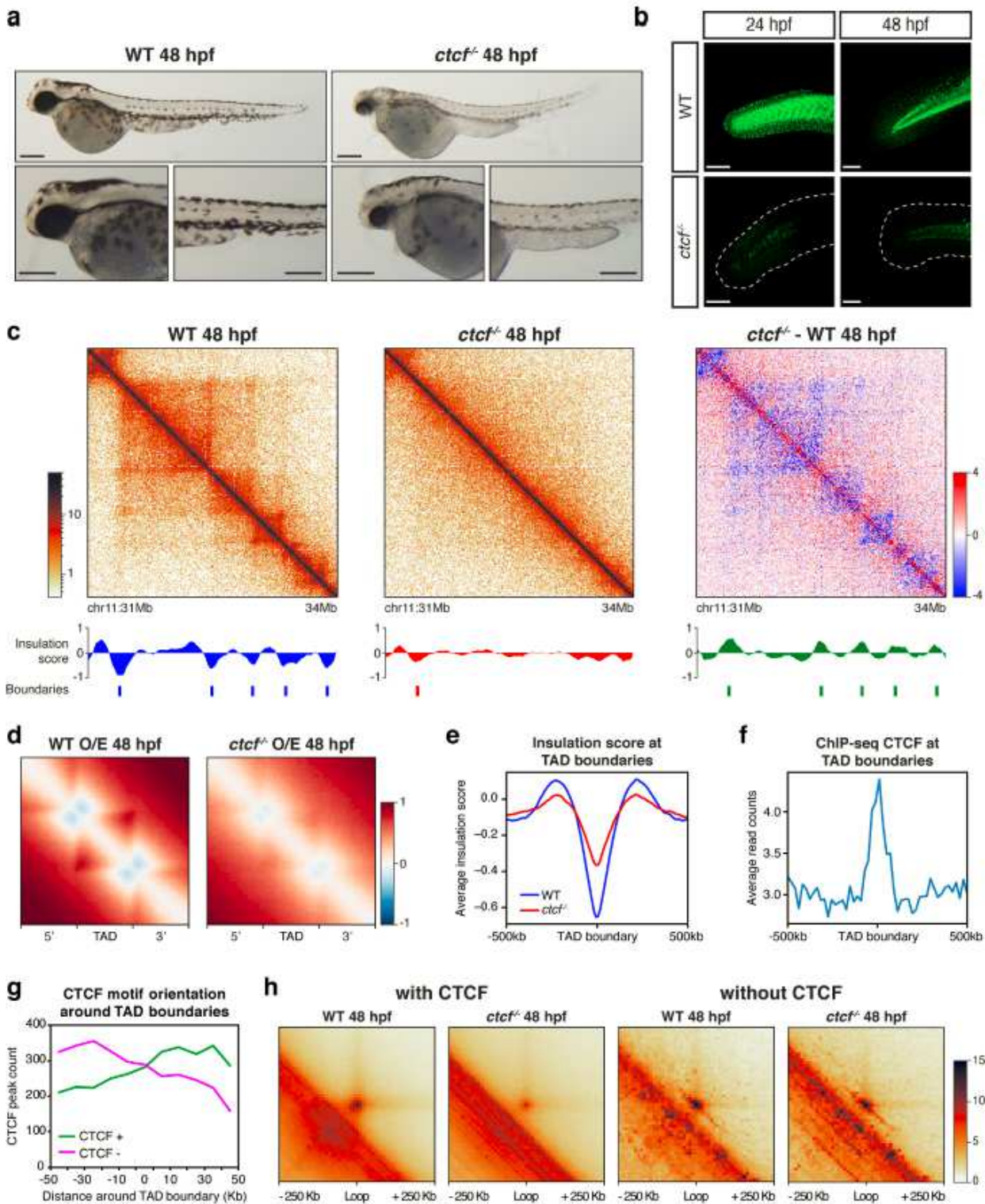


Figure 1

Knockout of *ctcf* in zebrafish embryos disrupts chromatin structure. **a**, Pictures of wild-type (WT) and *ctcf*^{-/-} zebrafish embryos at 48 hours post fertilization (hpf) showing mutant phenotypes, including reduced size of head and eyes, heart edema and defective pigmentation. Scale bars represent 250 μ m. **b**,

Whole-mount embryo immunofluorescence of CTCF in WT and *ctcf*^{-/-} zebrafish embryos at 24 and 48 hpf showing the absence of this protein in the tail and fin fold in knockout mutants. Scale bars represent 100 μm . c, HiC normalized contact maps at 10 Kb resolution from WT and *ctcf*^{-/-} zebrafish embryos, as well as the difference between them, at 48 hpf. A 3-Mb genomic region in chr11 is plotted, aligned with the insulation scores and the called topologically associating domain (TAD) boundaries. d, Aggregate analysis of observed/expected HiC signal in WT and *ctcf*^{-/-} embryos at 48 hpf for the 2,438 TADs called in WT embryos, rescaled and surrounded by windows of the same size. e, Average insulation score profiles of WT and *ctcf*^{-/-} zebrafish embryos at 48 hpf around the TAD borders called in the WT. f, Average CTCF ChIP-seq signal in WT embryos at 48 hpf around TAD boundaries. g, CTCF peak count of those peaks containing CTCF motifs located in the positive (CTCF +) or negative (CTCF -) strands around TAD boundaries, showing a clear preference for CTCF + motifs in the 3' side of the boundary and for CTCF - motifs in the 5' side of the boundary. h, Aggregate peak analysis of chromatin loops called by HiCCUPs with or without CTCF binding at 48 hpf.

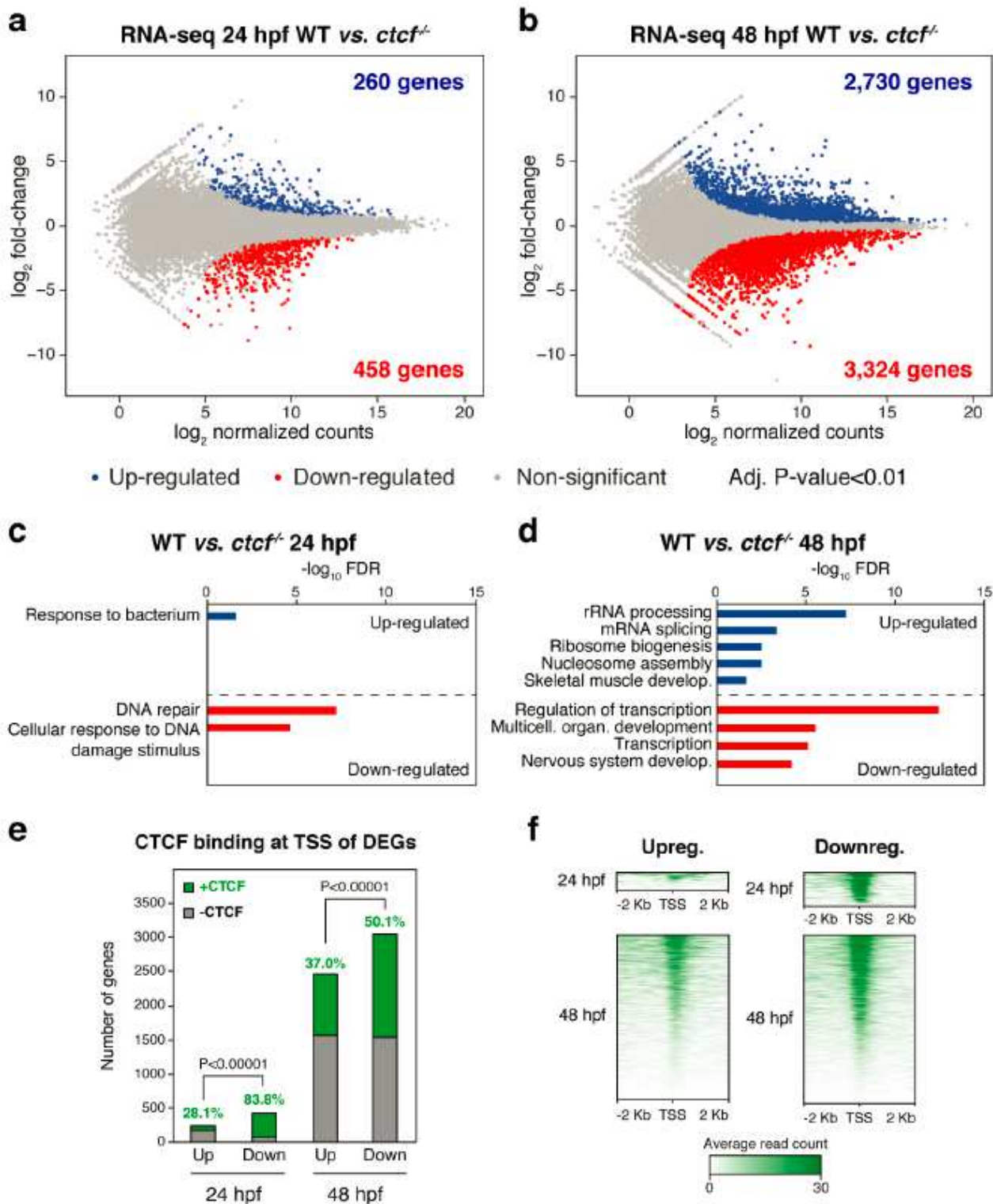


Figure 2

CTCF absence in zebrafish embryos leads to altered developmental gene expression. a-b, Differential analyses of gene expression between WT and *ctcf*^{-/-} embryos at 24 (a) and 48 hpf (b) from RNA-seq data ($n = 2$ biological replicates per condition). The \log_2 normalized read counts of WT transcripts versus the \log_2 fold-change of expression are plotted. Transcripts showing a statistically significant differential expression (adjusted P-value < 0.01) are highlighted in blue (up-regulated) or red (down-regulated). The

number of genes that correspond to the up- and down-regulated transcripts are shown inside the boxes. c, d, Gene Ontology (GO) enrichment analyses of biological processes for up- and down-regulated genes in *ctcf*^{-/-} embryos at 24 (c) and 48 hpf (d). Terms with a false discovery rate (FDR) < 0.05 are shown and considered as enriched. e, Number of differentially expressed genes (DEGs) at 24 and 48 hpf showing (green) or not (grey) CTCF binding at their transcription start sites (TSSs). f, Heatmaps showing CTCF ChIP-seq signal around the TSS of DEGs at 24 and 48 hpf.

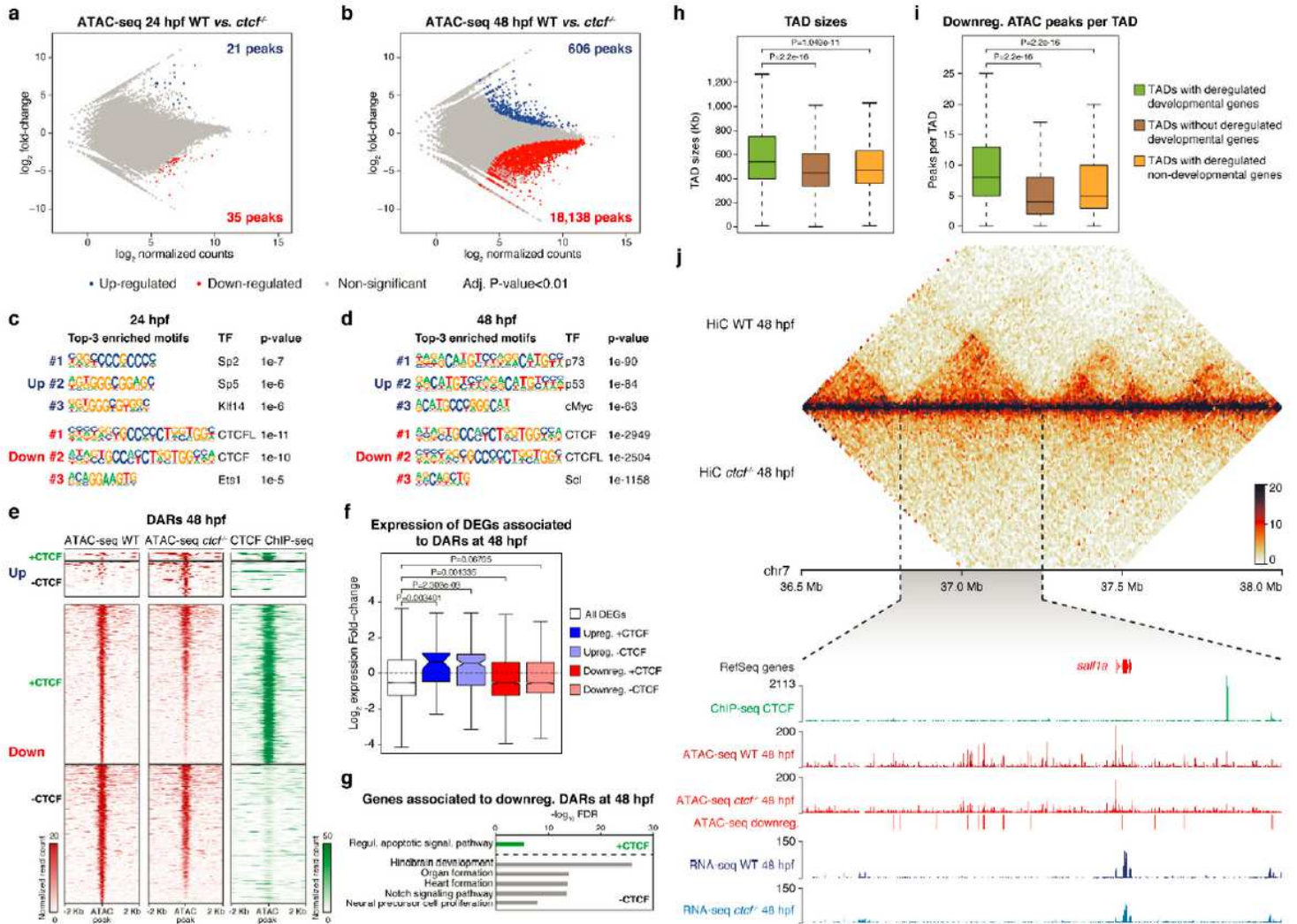


Figure 3

CTCF promotes chromatin accessibility at developmental cis-regulatory elements. a-b, Differential analyses of chromatin accessibility between WT and *ctcf*^{-/-} embryos at 24 (a) and 48 hpf (b) from ATAC-seq data (n = 2 biological replicates per condition). The log₂ normalized read counts of WT ATAC peaks versus the log₂ fold-change of accessibility are plotted. Regions showing a statistically significant differential accessibility (adjusted P-value < 0.01) are highlighted in blue (up-regulated) or red (down-regulated). The number of peaks that correspond to the up- and down-regulated sites are shown inside the boxes. c-d, Motif enrichment analyses for the up- and down-regulated ATAC peaks in *ctcf*^{-/-} embryos at 24 (c) and 48 hpf (d). The 3 motifs with the lowest p-values are shown for each case. e, Heatmaps plotting normalized ATAC-seq signal in WT and *ctcf*^{-/-} embryos at 48 hpf (red), as well as CTCF ChIP-seq

signal (green), for the differentially accessible regions (DARs) from (b) overlapping or not with CTCF peaks. f, Box plots showing the expression fold-change in *ctcf*^{-/-} embryos at 48 hpf of all DEGs or only those associated with up-regulated or down-regulated DARs, overlapping or not with CTCF sites. Center line, median; box limits, upper and lower quartiles; whiskers, 1.5x interquartile range; notches, 95% confidence interval of the median. Statistical significance was assessed using the Wilcoxon's rank sum test. g, GO enrichment analyses of biological processes for the genes associated with down-regulated DARs in *ctcf*^{-/-} embryos at 48 hpf, overlapping or not with CTCF sites. GO terms showing an FDR < 0.05 are considered as enriched. h-i, Box plots showing the TAD sizes (h) and the number of down-regulated DARs per TAD (i) for TADs containing developmental miss-regulated genes, TADs not containing developmental miss-regulated genes and TADs containing only non-developmental miss-regulated genes. Center line, median; box limits, upper and lower quartiles; whiskers, 1.5x interquartile range. Statistical significance was assessed using the Wilcoxon's rank sum test. j, Top, heatmaps showing HiC signal in WT and *ctcf*^{-/-} embryos at 48 hpf in a 1.5-Mb region of chromosome 7. Bottom, zoom within the *sall1a* TAD showing UCSC Genome Browser tracks with CTCF ChIP-seq, ATAC-seq at 48 hpf in WT and *ctcf*^{-/-} embryos, ATAC-seq down-regulated peaks and RNA-seq at 48 hpf in WT and *ctcf*^{-/-} embryos. The *sall1a* gene is shown in red because it is down-regulated.

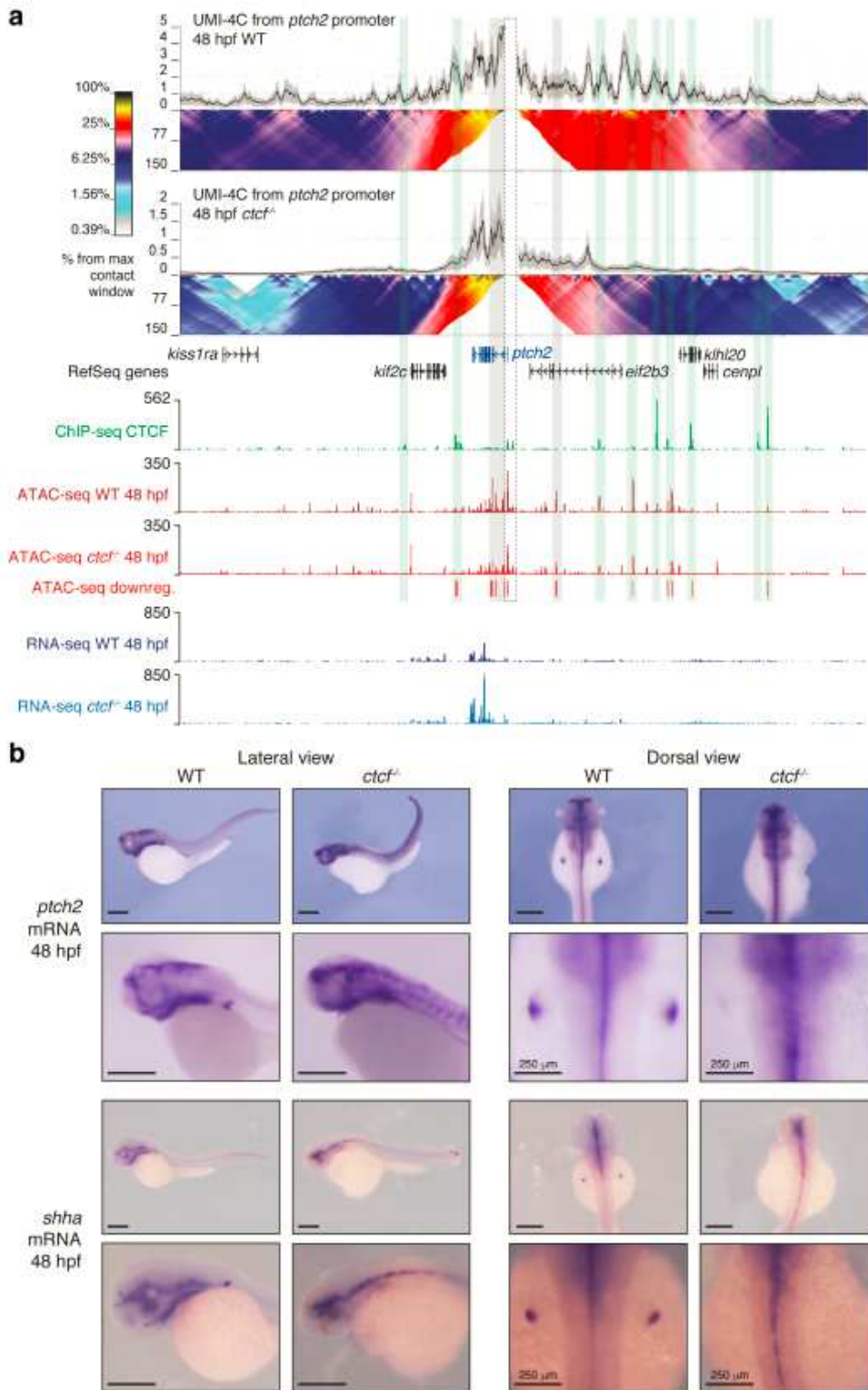


Figure 4

CTCF is required to sustain the regulatory landscapes and complex expression patterns of developmental genes. **a**, Top, UMI-4C assays in WT and *ctcf*^{-/-} embryos at 48 hpf using the *ptch2* gene promoter as a viewpoint. Black lines and grey shadows represent the average normalized UMI counts and their standard deviation, respectively. Domainograms below UMI counts represent contact frequency between pairs of genomic regions. Bottom, UCSC Genome Browser tracks with CTCF ChIP-seq, ATAC-seq at 48 hpf in WT

and *ctcf*^{-/-} embryos, ATAC-seq down-regulated peaks and RNA-seq at 48 hpf in WT and *ctcf*^{-/-} embryos. The *ptch2* gene is shown in blue because it is up-regulated. A dotted-line square represents the restriction fragment containing the *ptch2* gene promoter that is used as a viewpoint; green shadows highlight CTCF sites and grey shadows highlight down-regulated ATAC-peaks without CTCF binding. b, Whole-mount in situ hybridization of the *ptch2* and *shha* genes in WT and *ctcf*^{-/-} embryos at 48 hpf. Left, lateral view; right, dorsal view. Scale bars represent 500 μ m, unless indicated.